https://doi.org/10.5194/egusphere-2026-3066
Preprint. Discussion started: 11 June 2026

Eddy covariance measurements of nitrogen dioxide exchange at a grazed savanna grassland in South Africa

Tamryn Hamilton[1], Kerneels Jaars[1,2*], Pieter G. van Zyl[1], Mika Aurela[3], Marcellin Adon[4], Johan P. Beukes[1], Miroslav Josipovic[1], Gregor T. Feig[5,6], Markku Kulmala[7], Lauri Laakso[1,3], and Ville Vakkari[1,3]

[1]Atmospheric Chemistry Research Group, Chemical Resource Beneficiation, North-West University, Potchefstroom, South Africa
[2]Department of Chemistry and Polymer Science, Stellenbosch University, Stellenbosch, South Africa
[3]Finnish Meteorological Institute, Helsinki, Finland
[4]Laboratoire des Sciences et Technologie de l'Environnement (LSTE), Université Jean Lorougnon Guédé, Daloa, Côte d'Ivoire
[5]South African Environmental Observation Network, Pretoria, South Africa
[6]Department of Geography, Geoinformatics and Meteorology, University of Pretoria, Pretoria, South Africa
[7]Institute for Atmospheric and Earth System Research, University of Helsinki, Helsinki, Finland

Correspondence to: Kerneels Jaars (kjaars@sun.ac.za)

Abstract. South Africa is a global hotspot for anthropogenic atmospheric NO_2, where emissions from the industrialised Mpumalanga Highveld influence air quality across the southern African region. In the atmosphere, NO_2 is a key player in oxidative chemistry and contributes to particulate nitrate formation and the biogeochemical nitrogen cycle through deposition. At the same time, various ecosystem processes act as sources and sinks of NO and NO_2. The net result of these factors implies differences in the ecosystem scale flux of NO_2. Here we perform the first-ever high-resolution NO_2 measurements with a quantum cascade laser (QCL) instrument in a grazed African savannah landscape from 2015 to 2020. Micrometeorological eddy covariance measurements were used to quantify the NO_2 flux and explore temporal trends at diurnal, monthly, seasonal and interannual scales. Our findings highlight the variability of NO_2 flux within this system, with notable interannual change observed at both monthly and hourly scales. Seasonal differences in NO_2 flux and deposition velocity were strongly linked to the rainfall season, with negligible differences between dry season months. Diurnal flux trends peaked during daylight hours, with consistently low NO_2 flux during nighttime. These findings contribute to our understanding of near-surface atmospheric NO_2 dynamics in arid landscapes and, for the first time, can be used to estimate ecosystem-scale compensation point of NO_2.

1. Introduction

The oxidised forms of reactive atmospheric nitrogen, i.e. nitric oxide (NO) and nitrogen dioxide (NO_2) (together referred to as NO_x), have a strong influence on the oxidative capacity of the atmosphere through their contribution to the photochemical

https://doi.org/10.5194/egusphere-2026-3066
Preprint. Discussion started: 11 June 2026

formation of the hydroxyl radical (OH^-) in the atmosphere (Fowler et al., 2020). It is estimated that atmospheric photochemistry results in 100 $Tg.N.yr^{-1}$ returned globally to the surface through wet and dry deposition (Dentener et al., 2006; Duce et al., 2008). Wet deposition refers to the removal of atmospheric pollutant species through precipitation, whilst dry deposition refers to the gravitational settling of particles. Although the removal of NO_x from the atmosphere improves air quality, the spatial and temporal resolution associated with its deposition is not homogeneous (Dentener et al., 2006; Schwede et al., 2018; Zhou et al., 2021), but it is widely associated with high ambient concentrations (Lestari et al., 2003; Mariraj Mohan, 2016). Atmospheric dry deposition processes of NO_x are influenced by a combination of local and regional factors, which include climate (Borer and Stevens, 2022; W. Chen et al., 2023; Hertel et al., 2011), geophysical features (Cheng et al., 2013; Kopáček et al., 2012; Weathers et al., 2006), landcover (Zhang et al., 2009, 2003), economic activities (Jiang et al., 2024; Vizcaino and Lavalle, 2018) and legislation (Jiang et al., 2024; Shang et al., 2024). Regions affected by high NO_2 deposition are broadly associated with surface acidification (Lu et al., 2014; Stevens et al., 2011) resulting in biodiversity loss (de Vries et al., 2011) with changes in nitrogen deposition rates having variable effects on the environment (de Vries et al., 2011; Jiang et al., 2024; Stevens et al., 2011; Zhou et al., 2021). These impacts and the complex local- to regional-scale processes driving them contribute significantly to human and environmental health and represent a global focus area defined by the World Meteorological Organisation (WMO) Global Atmosphere Watch (GAW) (World Meteorological Organization, 2017) in support of the United Nations (UN) Agenda 2030.

Developments in our understanding of terrestrial nitrogen cycling incorporate multiple scientific disciplines to better understand the complex dynamics within landscapes that contribute to biosphere-atmosphere exchange processes. Multiple highly focused studies contribute to this body of knowledge, often quantifying nitrogen deposition interactions at various spatial scales with mass and energy transfers broadly termed fluxes. The methodological approaches of these studies vary, but can be generally defined as leaf-level measurements (ELLER and SPARKS, 2006; Gut et al., 2002; Sparks et al., 2001; Teklemariam and Sparks, 2006), chamber measurements (Behera and Sharma, 2011; Breuninger et al., 2013, 2011; Delaria et al., 2018) and landscape-level measurements (Grace et al., 2006; Horii et al., 2004; Min et al., 2014; Stella et al., 2013) which form a nested knowledge system that facilitates upscaling and interpretation. A major determinant of dry deposition is the uptake potential of the surface governed by surface resistance principles (Hicks et al., 1987; Wesely, 2007, 1989; Zhang et al., 2003), which quantify the attraction of gaseous particles towards an accumulation surface. Multiple parameters play a role, with the most important including near-surface turbulence, type of surface, wetness of the surface and overall solubility of the dry deposition species (Zhang et al., 2003). In the case of NO_2, multiple resistance modelling efforts were found to be ineffective (Hicks and Matt, 1988) and required the inclusion of plant physiology in the form of stomatal interactions (Chaparro-Suarez et al., 2011a; Geßler et al., 2002; Teklemariam and Sparks, 2006). In addition, soil processes and subsurface biota (Bowman et al., 2008; Goulding et al., 1998; Li et al., 2021) can emit NO, which in the presence of ozone (O_3) and

https://doi.org/10.5194/egusphere-2026-3066
Preprint. Discussion started: 11 June 2026

sunlight forms NO_2 (Wada et al., 2023). These ecosystem dynamics can be accounted for as either amplifying or mediating the uptake of dry deposition by factoring in local ambient conditions. (Deng et al., 2019). However, these local-scale dynamics require in-depth knowledge and are thus not often incorporated into nitrogen budgets (Wu et al., 2018).

More recently, many inferential modelling studies incorporate inferential model parameterizations into satellite imagery datasets in order to inform on large-scale atmospheric dry deposition (Cheng et al., 2013; Jia et al., 2016; Nowlan et al., 2014; Zhang et al., 2003; Zhou et al., 2021). However, these inferential model validations are limited by high-resolution flux measurement availability concentrated in North American and European landscapes (Giardina et al., 2019; Saylor et al., 2019; Zhang et al., 2009) with an absence of tropical and subtropical regions. This becomes important considering that tropical and sub-tropical systems dominate global trends for net primary production (Ahlström et al., 2015; Grace et al., 2006) and represent 50% of the African land surface area (Wu et al., 2018). The absence of representative validation datasets for African landscapes introduces uncertainty into satellite and model outputs, where these data are readily utilized to overcome deficits (Valentini et al., 2014). More importantly, many assumptions have to be made to produce quantifiable thresholds, such as critical loads (Josipovic et al., 2011) to interpret environmental responses and assess overall ecosystem resilience. These uncertainties, coupled with temperature extremes and drought conditions (Allan et al., 2023) anticipated from climate change, paint a vague and variable future for widely expected increases in nitrogen deposition (Bleeker et al., 2011).

In this study, we perform the first-ever high-resolution micrometeorological measurements of NO_2 at a regional background site in South Africa, a global hotspot for NO_2 emissions produced by coal-fired energy production and industry emissions clustered in the Highveld region. However, the South African landscape has limited flux measurements with no prior studies directly quantifying landscape-level fluxes of NO_2. We aim to explore NO_2 flux and investigate if a compensation point, i.e. a concentration where NO_2 net exchange levels out (Conrad, 1994), can be determined at ecosystem scale in a data-deficient region previously characterised by short-term, inferentially modelled deposition (Held and Mphepya, 2000).

2. Materials and methods

2.1. Site description

Eddy covariance fluxes of NO_2 together with an extensive set of supporting measurements were conducted at the Welgegund Atmospheric Measurement Station (WAMS) (26°34'10 "S, 26°56'21 "E, 1480 m a.s.l.; http://www.welgegund.org), a regional background site in South Africa, for which detailed site descriptions have been presented in numerous papers (e.g. Jaars et al., 2014, 2016, 2018; Räsänen et al., 2017). In brief, the research site is approximately 140 km southwest of the Johannesburg-Pretoria megacity and is frequented impacted by aged pollution plumes (Beukes et al., 2013; Kok et al., 2021; Laban et al., 2018; Lourens et al., 2011) facilitated by regional anticyclonic circulation (Freiman and Piketh, 2003; Tyson et al., 1996). Air

https://doi.org/10.5194/egusphere-2026-3066
Preprint. Discussion started: 11 June 2026

masses measured at Welgegund, as indicated in Figure 1, combines emissions from various source regions in the north-eastern interior of South Africa, which include the Johannesburg-Pretoria megacity, the heavy-industry dominated Vaal Triangle, the western Bushveld Complex and the eastern Mpumalanga Highveld (Beukes et al., 2013; Lourens et al., 2011; Venter et al., 2012). However, the site is also impacted by relatively clean air masses from the north-northwest to the south-southwest sector (Kai et al., 2022; Venter, 2020).

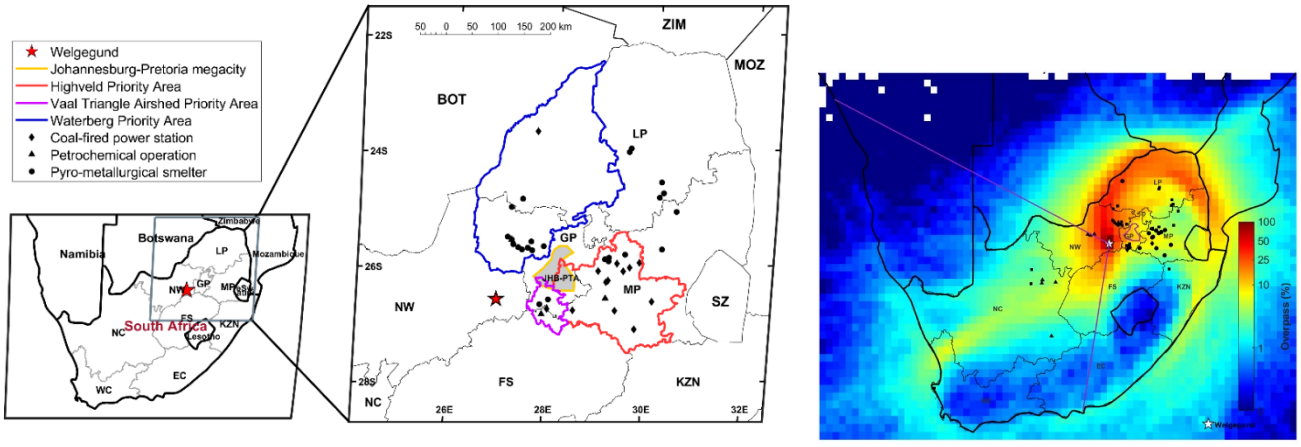

Figure 1: Map of the study site (red star) in South Africa showing relevant emissions sources (black points) in the industrialized North-Eastern sector (left). Overlay back trajectory map (right) for air masses sampled at Welgegund (white star) over the entire monitoring period (2015-2020). Dark red fill indicates the highest percentage back trajectory overpass and dark blue the lowest. Purple lines show the Western and South-western quadrant associated with relatively clean air masses. The location of large emission point sources in the South African interior is also indicated.

The WAMS is situated on the border of the grassland and savanna biomes (Figure 1). The immediate landscape consists of a mosaic of long grass, thorn shrubland and savanna patches (Jaars et al., 2016; Räsänen et al., 2017) that occur within the 80% cumulative flux footprint (324 m radius (Räsänen et al., 2017)). Agricultural croplands are located ~500m away from the site in the North-east and South-west directions of the instrument housing, with a dirt access road in the North-north-east direction. The site is periodically grazed by free-roaming cattle and sheep. For a detailed description of soil, vegetation and auxiliary meteorological parameters, see Jaars *et al.* (2014) and Räsänen *et al.* (2017).

Recent statistical analysis of local atmospheric temperatures (Van der Walt and Fitchett, 2020) classified different seasons of the South Africa region as summer from October to March, autumn from April to May, winter from June to July and spring from August to September, which will be adopted for the seasonal classification in this paper. The summer season is generally characterised by convective conditions and accounts for >80% of the annual rainfall with an overall increase in biomass during this period. Spring and autumn seasons have subtly cooler air temperatures. Winter is dominated by cool and dry conditions with prolonged low-level persistence of the planetary boundary layer (Gierens et al., 2019; Korhonen et al., 2014) and inversion

https://doi.org/10.5194/egusphere-2026-3066
Preprint. Discussion started: 11 June 2026

layers (Cosijn, 1996). The transition from autumn to the winter season also facilitates an overall reduction in biomass in the form of plant senescence, which can result in frequent fires from June to December (Archibald, 2010).

2.2. Data acquisition and ancillary measurements

The eddy covariance (EC) method provides continuous, ecosystem-scale measurements of turbulent exchanges of mass and energy between ecosystems and the atmosphere (Aubinet et al., 2012; Burba and Anderson, 2010). The method is widely used to measure fluxes of carbon dioxide (CO_2) and water vapour (H_2O), and has also been applied in several studies to quantify exchanges of reactive nitrogen species such as NO_2 (Horii et al., 2004; Min et al., 2014; Stella et al., 2013). In these types of measurements, wind speed, wind direction, and gaseous concentrations within a parcel of air as it passes over a gas sensor are measured. At the WAMS, EC measurements for CO_2, H_2O, sensible heat, and momentum have been conducted since September 2010 using an enclosed-path LI-7000 (LI-COR, Inc., USA) gas analyser coupled with an USA-1 (METEK GmbH, Germany) 3D sonic anemometer, following a configuration similar to that used by Aurela *et al.* (2009) and Räsänen *et al.* (2017).

Fast-response Quantum Cascade Laser (QCL) spectroscopy is well suited for integration with EC flux systems for trace gas flux measurements (Li et al., 2013; Tuzson et al., 2010) and has been employed in multiple studies on NO_x exchange in forest (Horii, 2002; Horii et al., 2004, 1999; Raivonen et al., 2009) and meadow (Stella et al., 2013) ecosystems. In February 2015, a fast-response Aerodyne dual-laser QCL was installed at WAMS to measure surface-atmosphere NO_2 exchange. The instrument utilised two simultaneous sampling lasers, with one specifically configured to probe the fundamental absorption band of NO_2 and H_2O (Alpes Lasers #sbcw3877 DN, v=6.2µm, λ= ~1604 cm^{-1}). The QCL was coupled with the sonic anemometer and operated at a sampling frequency of 10 Hz. Air was drawn through a 20 m heated PFA Teflon inlet tube (inner diameter 4 mm) at a flow rate of 6.5 L min^{-1} from an inlet located 9 m above ground level, via a PTFE filter, similar to the configuration described by Räsänen et al. (2017).

The QCL was housed within a climate-controlled and was subjected to weekly instrumental checks. During the data collection period, the QCL underwent two factory calibrations, including laser re-alignments, which resulted in extended data gaps. Raw 10 Hz data were logged on a dedicated PC to ensure stable data acquisition at high frequency (Gerdel et al., 2017) with TDL Wintel software (Aerodyne, USA). High-frequency data underwent additional data-filtering to account for QCL laser performance. Data screening of 30-minute flux data applied a friction velocity threshold (u_* >0.2 ms^{-1}) (Papale et al., 2006), and excluded extreme NO_2 concentrations (>50 ppb) and poor stationarity (Foken and Wichura, 1996).

Previously, plant NO_2 exchange has been studied mostly at leaf or branch level (Farmer and Cohen, 2008; GESSLER et al., 2000; Gut et al., 2002; Ke et al., 2025). At this scale, the concept of "compensation point" has been developed, i.e. a

https://doi.org/10.5194/egusphere-2026-3066
Preprint. Discussion started: 11 June 2026

concentration where NO_2 sources and sinks balance each other (Breuninger et al., 2011; Conrad, 1994; Raivonen et al., 2009). With the compensation point concentration C_P, the NO_2 flux (F) can be expressed as:

$$F = -v_d(C - C_P) \quad , \quad (1)$$

Where (v_d) are deposition velocity and C is the instantaneous ambient atmospheric concentration (e.g. Breuninger et al., 2012).

Ancillary measurements continuously performed at the station include ambient trace gas and meteorological measurements (Appendix) sampled every minute, with the 15-minute averages recorded. These ancillary measurements have been well described by other studies (e.g. Laakso *et al.*, 2012; Jaars *et al.*, 2014, 2016; Vakkari *et al.*, 2014; Räsänen *et al.*, 2017).

The cumulative effect of instrumental and micrometeorological filtering resulted in a final data recovery of approximately 36.6% (Table 1; Figure 2a), consistent with QCL performance reported by Gerdel *et al.* (2017). Cross-validation of co-located H2O concentration measurements from the QCL and LI-7000 yielded a near-perfect linear fit (adjusted $R^2 > 0.99$, $p < 10^{-10}$) (Fig. 1b) for a representative subsample of $n = 1440$ intervals, confirming the instrumental synchronicity required for coupled EC systems. The final dataset exhibited a 60:40 daytime-to-night-time split, reflecting the well-known increase in nocturnal data loss under stable atmospheric conditions (Thomas and Foken, 2002; Papale et al., 2006; Räsänen et al., 2017).

Table 1: Data recovery and quality control (QC) filtering statistics for the WAMS eddy covariance (EC) system (2015-2020).

Filtering step	Description	Total points	Recovery (%)	Day (%)	Night (%)
Total record	Full study period (30-min intervals)	93 685	100	—	—
Instrumental QC	QCL diagnostics (power, laser, spectral fit)	48 578	51.9	49.6	50.4
Post-processing	u_* filtering, stationarity, and concentration limits	34 239	36.6	60.1	40
Final valid record	Data used for flux analysis	34 239	36.6	60.1	40

https://doi.org/10.5194/egusphere-2026-3066
Preprint. Discussion started: 11 June 2026

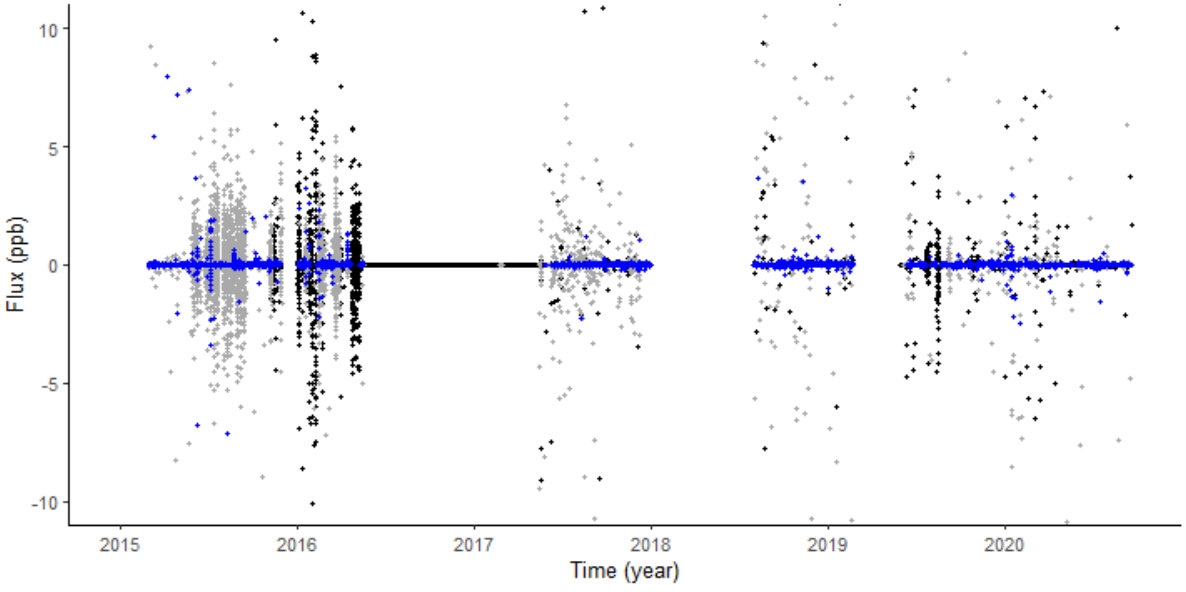

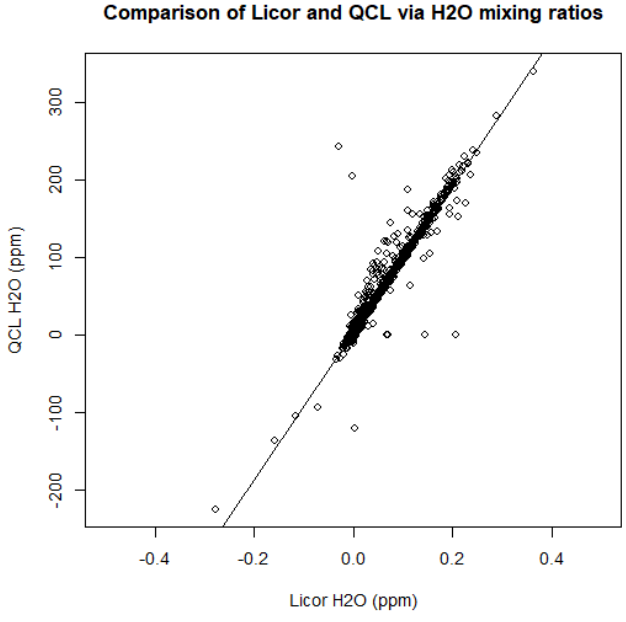

160 **Figure 2: Quality control and instrumental performance of the eddy-covariance (EC) system (2015-2020). (a) Time series of NO_2 flux data illustrating the data-filtering hierarchy: raw observations (grey), exclusions due to quantum cascade laser (QCL) diagnostic performance (black), and periods removed based on standard EC post-processing and stationarity criteria (blue). Data gaps are attributed to instrument downtime and scheduled factory calibrations. (b) Linear regression between H_2O concentrations (ppb) measured by the QCL and the LI-COR gas analyser for a representative sample (n = 1440), demonstrating instrumental cross-**
165 **validation and stability throughout the observation period.**

https://doi.org/10.5194/egusphere-2026-3066
Preprint. Discussion started: 11 June 2026

2.3. Inferentially modelled NO_2 deposition velocity

To complement the micrometeorological measurements, a state-of-the-art dry deposition inferential model of Zhang et al. (2003), adapted by Adon *et al.* (2013) to African ecosystems was used to assess the v_d. The model utilises a big-leaf resistance framework to estimate v_d based on independently measured ambient NO_2 concentrations, remotely sensed meteorological parameters, and specific land-use classification. This approach generated 3-hour monthly averages of v_d for the 2015-2020 study period, providing a robust baseline for comparing the eddy covariance results with modelled estimates.

Accurate parameterisation of the canopy structure is critical for inferential modelling in savanna systems. Vegetation sampling at the site by Räsänen *et al.* (2017), indicated that the Leaf Area Index (LAI) within the footprint of the site ranged from 0.4 to 2.3 $m^2\ m^{-2}$. Observed LAI measurements corresponded with the more conservative MODIS averaged LAI, which ranged from 0.3 to 1.5 $m^2\ m^{-2}$ (2000-2021). The observed mean LAI of 1.2 $m^2\ m^{-2}$ was found to correspond most accurately with the Zhang *et al*. (2003) land-use classification (LUC) for short grass and forbs. Consequently, this LUC was selected to provide the aerodynamic and surface resistance parameters necessary to resolve the v_d across the inter-annual study period.

3. Results and discussion

3.1. Meteorological conditions

The meteorological time series were synchronised with periods of valid eddy covariance NO_2 flux measurements to ensure that environmental drivers and exchange processes were directly comparable (Figure 3). Consequently, the statistics presented here describe the meteorological envelope under which NO_2 fluxes were observed rather than the full climatological conditions at the site. In Figure 3, daily median values in the time-series panels (black lines), are intentionally broken where data gaps occur in order to avoid visual interpolation across periods without observations. Cumulative daily precipitation for the study period is further detailed in Figure 4.

Local meteorological forcing plays a dominant role in regulating surface–atmosphere exchange of reactive nitrogen at the site, driven by rapid photochemical cycling and strong coupling between soil and boundary-layer dynamics. Figure 3 presents the temporal evolution of these drivers, arranged to highlight the transition from radiative forcing to surface response: (a) global radiation (G_r), (b) air temperature (T_a), and (c) soil temperature at 5 cm depth (ST_{5cm}) establish the thermal regime, followed by (d) soil heat flux (SHF) and (e) relative humidity (RH). The hydrological state is captured by (f) precipitation and (g) soil moisture (SM_{5cm}) at 5 cm depth, which directly precedes the resulting (h) measured NO_2 flux. This aligned vertical structure highlights the synchronisation between episodic moisture pulses, thermal cycles, and the subsequent trace gas exchange observed between 2015 and 2020.

https://doi.org/10.5194/egusphere-2026-3066
Preprint. Discussion started: 11 June 2026

G_r exhibited a wide dynamic range (0-1229 W m^{-2}; mean 469 W m^{-2}; CV ≈ 0.70), indicating strong radiative forcing typical of semi-arid Highveld conditions. T_a averaged 18.5 ± 6.8 °C and was closely coupled with ST_{5cm} (mean 20.9 ± 8.9 °C; r = 0.88), suggesting strong thermal linkage between the atmosphere and near-surface soil layers. Soil heat flux showed the largest relative variability (CV = 3.34), with a negative median (-5.7 W.m^{-2}) and pronounced bidirectional extremes (-153 to 253 W.m^{-2}) that were consistent with alternating nocturnal cooling and daytime conductive heating. The strong relationship between G_r and SHF (r = 0.81) further indicates that radiative forcing largely governs energy redistribution at the soil-atmosphere interface.

Hydrothermal conditions were characterised by substantial variability associated with episodic precipitation and seasonal moisture availability. RH averaged 45.6 % (median = 40.6 %) and displayed clear wet- and dry-season contrasts (50.6 % vs. 35.3 %), while SM_{5cm} remained generally low (mean = 0.114 m^3 m^{-3}) with only modest seasonal differences (wet median 0.13 m^3 m^{-3}; dry median 0.09 m^3 m^{-3}). RH exhibited negative correlations with T_a (r = -0.54) and SHF (r = -0.49), indicating that periods of enhanced surface heating coincided with reduced atmospheric moisture. In contrast, SM_{5cm} showed weak associations with radiative variables, suggesting that soil moisture variability was largely controlled by intermittent precipitation events rather than sustained solar forcing. Rainfall intensity was generally low (mean = 0.0496 mm h^{-1}; median = 0 mm h^{-1}), and only six heavy rainfall events (> 10 mm h^{-1}) were observed during the study period. Annual rainfall totals within the flux-synchronised record ranged from approximately 53 mm to 143 mm, and cumulative precipitation curves displayed a step-like structure characteristic of pulse-driven hydrological regimes. Such episodic wetting events are consistent with short-lived increases in soil microbial activity and transient NO_x production.

The combined influence of radiative forcing and pulse-driven hydrothermal variability establishes a dynamic surface–atmosphere coupling regime that shapes the timing of NO_2 exchange. Periods of elevated radiation and positive soil heating are associated with unstable boundary-layer conditions and enhanced turbulent mixing, whereas nocturnal cooling and post-rainfall conditions favour more stable stratification. Because the meteorological record is limited to intervals with valid flux measurements, the analysed conditions emphasise periods of active exchange rather than the full range of background meteorological states. The observed coupling between G_r, SHF, and temperature therefore provides a physical context for interpreting the NO_2 flux behaviour shown in Figure 3, where peak daytime flux exchange coincides with enhanced mixing, and episodic responses following rainfall are consistent with moisture-induced microbial activation. These energy-balance and hydrothermal characteristics form the basis for the diurnal NO_2 flux analysis presented in the results section.

https://doi.org/10.5194/egusphere-2026-3066
Preprint. Discussion started: 11 June 2026

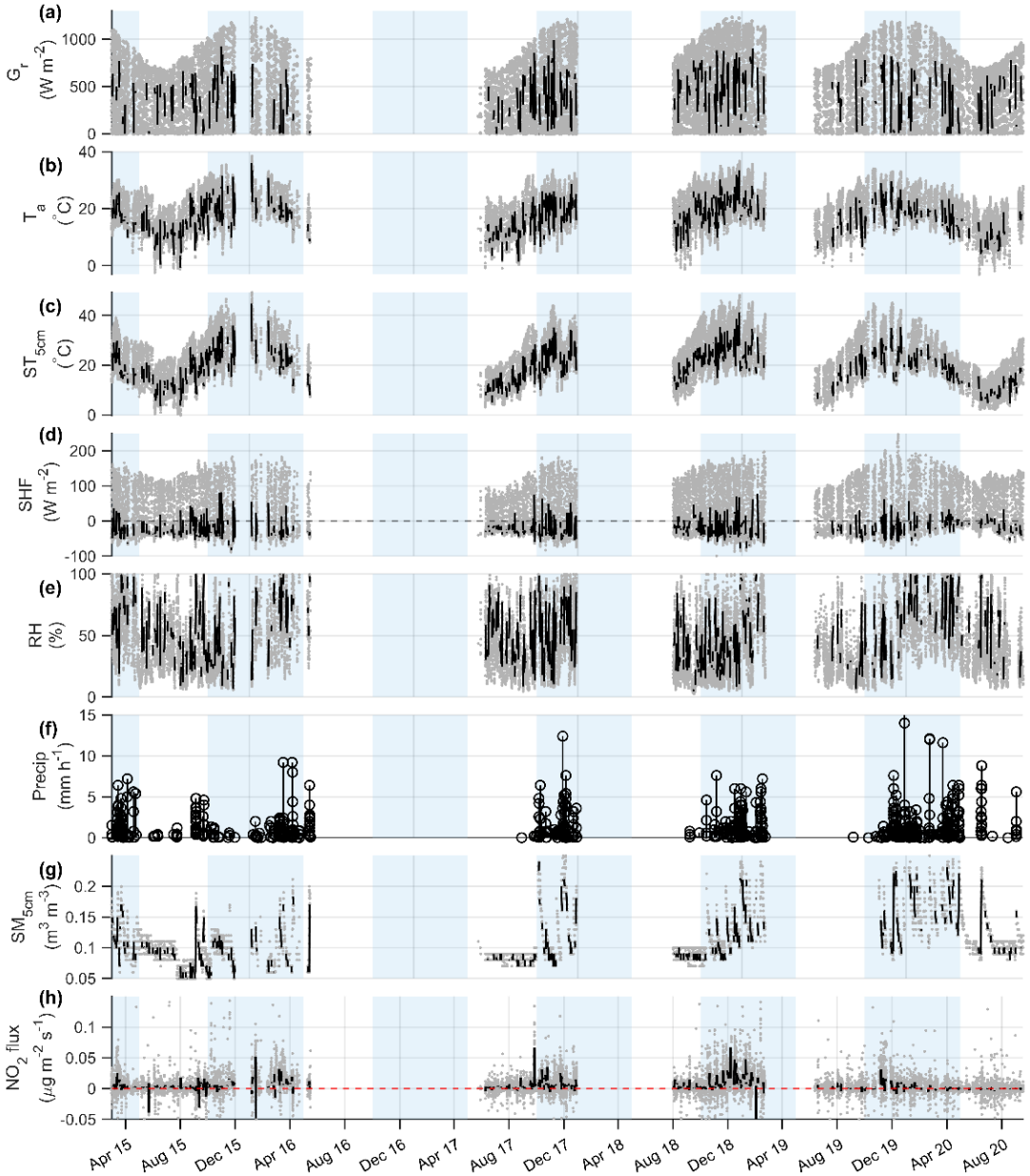

Figure 3: Time series of meteorological and land-surface variables at the site (2015–2020). Panels represent (a) global radiation (G_r), (b) air temperature (T_a), and (c) soil temperature at 5 cm depth (ST_{5cm}), (d) soil heat flux (SHF), (e) relative humidity (RH), (f) precipitation and (g) soil moisture (SM_{5cm}) at 5 cm depth, alongside the resulting (h) measured NO_2 flux. Grey markers denote half-hourly observations and black lines represent daily median values to emphasise seasonal variability. Shaded vertical bands indicate wet-season periods (October–April). The shared x-axis highlights the coherent seasonal evolution of atmospheric forcing, radiative energy, and soil hydrothermal conditions driving the observed NO_2 exchange.

https://doi.org/10.5194/egusphere-2026-3066
Preprint. Discussion started: 11 June 2026

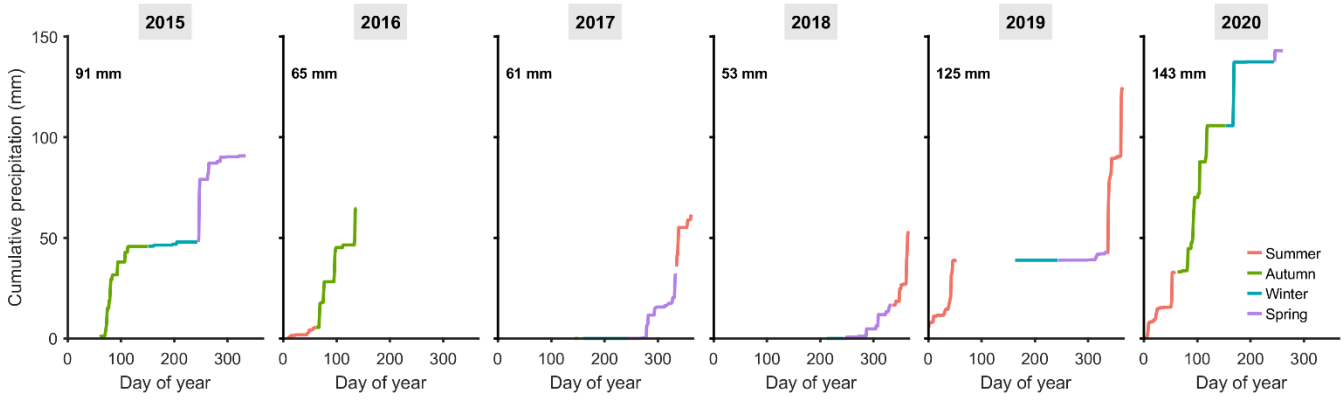

Figure 4: Cumulative precipitation at the site for the study period. Each panel represents an individual hydrological year, with cumulative rainfall (mm) plotted against day of year. Line colours indicate climatological seasons (summer: red; autumn: green; winter: blue; spring: purple). Annual totals are shown within each panel. The step-like structure reflects episodic rainfall events typical of the semi-arid savannah environment, with most accumulation occurring during the summer months and limited increases during winter. Differences in slope and timing between years highlight strong interannual variability in rainfall intensity, onset, and seasonal distribution.

3.2. NO_2 surface-atmosphere exchange

Net surface-atmosphere exchange of NO_2 was evaluated using 21 681 quality-assured, non-gap-filled flux observations measured between 2015 and 2020. Following post-processing and quality control, the dataset comprised a 60:40 distribution between daytime and nighttime measurements, indicating the commonly observed reduction in nocturnal data coverage due to low turbulence conditions (Papale et al., 2006; Räsänen et al., 2017; Thomas and Foken, 2002). Across the full observation period, NO_2 exchange exhibited pronounced bidirectional behaviour but was dominated by net emission, with 72.82 % (N = 15 788) of fluxes directed upward from the surface to the atmosphere, compared to 27.18 % (N = 5 893) representing deposition.

Half-hourly fluxes ranged from -4.23 to 5.58 $\mu g\ m^{-2}\ s^{-1}$, highlighting substantial temporal variability in surface-atmosphere exchange processes. The overall distribution was weakly skewed towards positive values, with a mean flux of 0.0058 $\mu g\ m^{-2}\ s^{-1}$, and a median of 0.0032 $\mu g\ m^{-2}\ s^{-1}$ (interquartile range, IQR = 0.0093 $\mu g\ m^{-2}\ s^{-1}$), indicating that episodic high-magnitude events contributed disproportionately to the mean exchange signal. Collectively, these statistics demonstrate that the measurement site functioned predominantly as a net source of NO_2 over the multi-year period, while retaining strong temporal variability across diurnal, seasonal, and interannual timescales.

https://doi.org/10.5194/egusphere-2026-3066
Preprint. Discussion started: 11 June 2026

3.2.1 Temporal variability of net NO_2 flux

i. Seasonal and interannual variability

Net NO_2 fluxes exhibited pronounced temporal variability across monthly, seasonal, and interannual timescales, reflecting the combined influence of meteorology, surface conditions, and regional pollution dynamics (Figure 7). Monthly box-and-whisker distributions revealed a persistent dominance of positive fluxes throughout most of the measurement period, indicating that the site generally functioned as a net source of NO_2 to the atmosphere. The highest median fluxes occurred during the summer months, particularly in January (0.0099 µg m^{-2} s^{-1}), November (0.0074 µg m^{-2} s^{-1}), and December (0.0072 µg m^{-2} s^{-1}), whereas substantially lower medians were observed during late autumn and winter, including April (0.0014 µg m^{-2} s^{-1}), June and July (0.0015 µg m^{-2} s^{-1}). Exceptions occurred in select months during 2020, i.e., July, August, and September, as well as in May 2017, when median fluxes dipped marginally below zero. These periods of net deposition were also characterised by relatively narrow IQRs, suggesting more stable surface-atmosphere exchange or increased stomatal resistance. The negative flux median for May 2017 could be attributed to the low number of flux observations for the month (N = 12), which occurred when the QCL instrument was reinstalled after calibration. These seasonal contrasts highlight the strong sensitivity of NO_2 exchange to environmental controls such as soil moisture, solar radiation, and boundary-layer development.

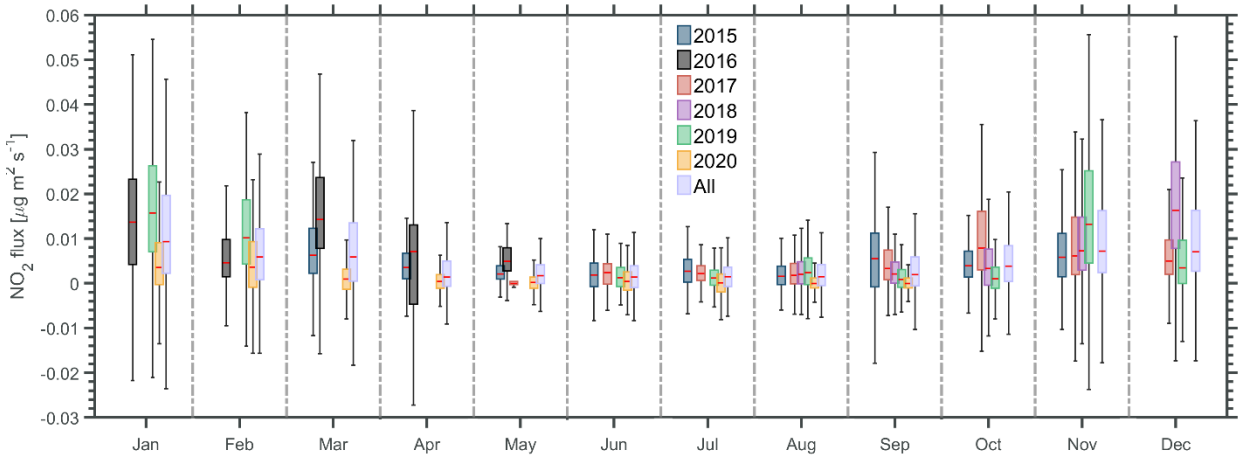

Figure 5: Monthly distributions of NO_2 fluxes presented as box-and-whisker plots for the period 2015-2020. Boxes represent the interquartile range (25th - 75th percentiles), the bold red line indicates the median, and whiskers extend to 1.5 × IQR. Fluxes are expressed in µg m^{-2} s^{-1}, where positive values denote net emission and negative values indicate deposition. Colours distinguish individual years, while the aggregated "All" category represents the combined dataset across all years.

https://doi.org/10.5194/egusphere-2026-3066
Preprint. Discussion started: 11 June 2026

Seasonal trends in the total NO_2 fluxes were pronounced, shifting from a highly active wet season to a suppressed flux regime during the winter months. During the wet season (October-April), emissions dominated, accounting for 77.8 % of flux observations, with a mean (median) flux of 0.0091 (0.0055) $\mu g\, m^{-2}\, s^{-1}$ and an IQR of 0.0127 $\mu g\, m^{-2}\, s^{-1}$. Similarly, during the dry season (May-September), emissions remained dominant at 66.98%, though the regime was significantly suppressed (mean = 0.0020 $\mu g\, m^{-2}\, s^{-1}$; median = 0.0017 $\mu g\, m^{-2}\, s^{-1}$, IQR = 0.0055 $\mu g\, m^{-2}\, s^{-1}$), with a higher proportion of deposition (43.02%) compared to the wet months. This transition resulted in a seasonal flux ratio of 4.55, indicating that NO_2 emission intensity is more than four times higher during the wet season. While many temperate or tropical ecosystems typically exhibit seasonal ratios between 1.5 and 2.0, this high ratio of 4.55 specifically points to the extreme seasonality of the South African Highveld and its "wet-hot" versus "dry-cold" contrast (Maritz et al., 2015). This shift towards weaker exchange during the dry season is consistent with reduced soil moisture availability, lower biological activity, and more stable atmospheric stratification typical of Highveld winter conditions (Freiman and Piketh, 2003; Segakweng et al., 2022). Despite these seasonal shifts, median fluxes remained predominantly positive across most months and years, reinforcing the persistence of a net emission regime at the site.

Analysis of interannual variability reveals a system defined by high year-to-year fluctuations and a strong dependence on the timing of rainfall relative to soil nitrogen availability. The highest annual mean (0.0132 $\mu g\, m^{-2}\, s^{-1}$) and median (0.0091 $\mu g\, m^{-2}\, s^{-1}$) were observed in 2016; however, these values coincide with the lowest data coverage of the study period (~6%), suggesting the 2016 statistics are likely biased by the chance capture of high-energy emission events rather than representing a sustained annual baseline. The most substantial within-year variability (highest IQR) was also recorded in 2016 (IQR = 0.0154 $\mu g\, m^{-2}\, s^{-1}$), followed by 2019 (IQR = 0.0125 $\mu g\, m^{-2}\, s^{-1}$). In contrast, the 2020 results provide a rare glimpse into the ecosystem's basal exchange mode. The transition to a negative annual mean flux (mean = -2.1×10^{-6} $\mu g\, m^{-2}\, s^{-1}$ and median = 0.0007 $\mu g\, m^{-2}\, s^{-1}$) signifies a fundamental shift in the system's state, where the site functioned as a net sink rather than a source. This deposition-dominated state in 2020 is a direct consequence of the data excluding the October to December rainfall onset. In the absence of these early wet season observations, the onset of the rainfall season and upward NO_2 pulses from re-wetted soils are missed. Leaving the annual mean to reflect an emission "starved" state dominated by dry deposition. This highlights the site's status as a net source as strictly dependent on the combined effect of precipitation and microbial activation. Moreover, this sensitivity is further reflected in the highest monthly ranges recorded in December 2018 (IQR = 0.0195 $\mu g\, m^{-2}\, s^{-1}$) and November 2019 (IQR = 0.0201 $\mu g\, m^{-2}\, s^{-1}$), which mark periods of high-frequency changes in surface emissions and rapid shifts in atmospheric stability during the wet-season transition.

The NO_2 exchange dynamic is further disrupted by high-magnitude, episodic events that deviate sharply from average conditions. Extreme positive fluxes, defined as those exceeding the 99th percentile threshold (0.0662 $\mu g\, m^{-2}\, s^{-1}$), occurred 217 times, with the most extreme positive flux being recorded on 8 April 2015 (5.58 $\mu g\, m^{-2}\, s^{-1}$). Similarly, 217 fluxes fell below

https://doi.org/10.5194/egusphere-2026-3066
Preprint. Discussion started: 11 June 2026

the 1st percentile threshold (-0.0439 µg m^{-2} s^{-1}), with the lowest flux of -0.0627 µg m^{-2} s^{-1} measured on 23 March 2015. The grouping of these extremes in early autumn suggest a pulse-reserve mechanism. During these periods, accumulated soil nitrogen is suddenly mobilised by late-season convective rainfall. Alternatively, rapid shifts in the planetary boundary layer height may trigger the venting of NO_2 previously trapped in the surface layer by winter-like temperature inversions. The April 2015 peak, sitting orders of magnitude above the mean, suggests that the long-term nitrogen budget of the Highveld is likely dictated by these rare, high-intensity interactions rather than steady-state exchange. These episodic bursts represent critical points of high-intensity coupling that likely govern the oxidative capacity of the regional troposphere.

ii. Diurnal variability

The diurnal patterns of NO_2 flux exhibited a clear seasonal variation, characterised by a predominantly unimodal structure with enhanced daytime emissions. As illustrated in Figure 6, the median diurnal trends, derived from hourly medians across all years, reveal a clear divergence from ambient NO_2 concentrations. While concentrations typically display a bimodal trend linked to morning and evening traffic peaks, NO_2 fluxes demonstrated an unimodal profile with positive hourly flux magnitudes and greater variability during daytime hours, peaking between 09:00 and 15:00. This behavior suggests that vertical exchange is not a reflection of the concentration gradient but is governed by an active interaction of biological source strength, photochemical activity, and convective boundary layer (CBL) evolution. Summer months represent the peak of this exchange intensity, with median diurnal magnitudes more than double those recorded in any other season. During this window, net emissions were observed in 79.4% of observations (N = 10435), yielding a mean flux of 0.0097 µg m^{-2} s^{-1} and an IQR of 0.0133 µg m^{-2} s^{-1}, with a right-skewed distribution.

https://doi.org/10.5194/egusphere-2026-3066
Preprint. Discussion started: 11 June 2026

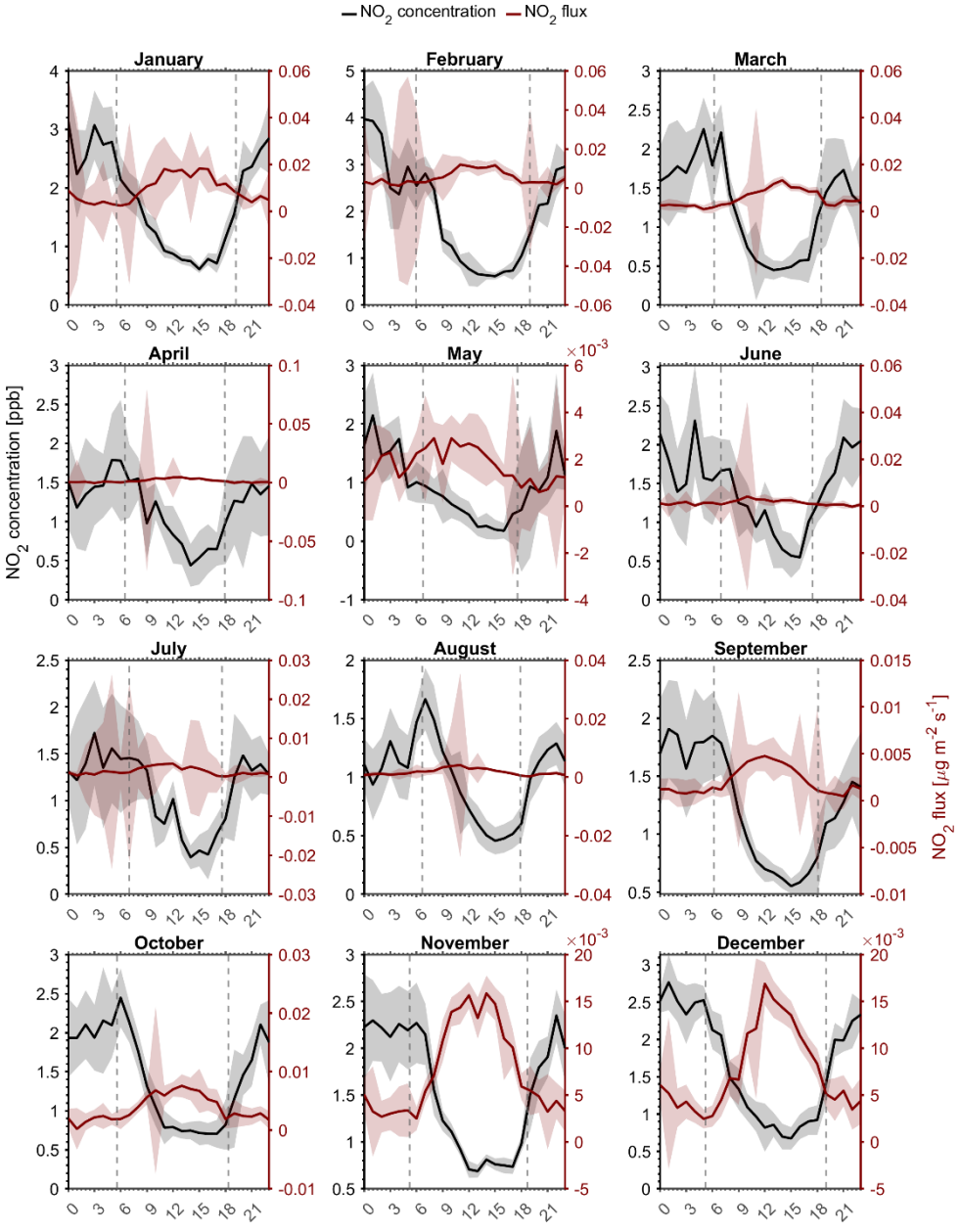

Figure 6: Mean diurnal cycles of NO_2 concentration (ppb; black line, left axis) and NO_2 flux (μg m^{-2} s^{-1}; red line, right axis) for each calendar month at the Welgegund measurement site from March 2015 to September 2020. Panels show monthly averages derived from half-hourly observations, with shaded envelopes indicating the standard error of the mean to illustrate variability in both concentration and exchange. Vertical dashed lines denote dynamically calculated local sunrise and sunset times, separating daytime and nocturnal boundary-layer regimes.

https://doi.org/10.5194/egusphere-2026-3066
Preprint. Discussion started: 11 June 2026

This intensification is mechanically driven by the Highveld's summer hydro-climatology. The influx of over 80% of the annual precipitation triggers a rapid transition in soil moisture content (5 cm), stimulating biogenic soil emissions in an otherwise water-limited environment (Feig et al., 2008; Stewart et al., 2008). These moisture-induced pulses, often associated with the Birch Effect, are further amplified by high global radiation and extended photoperiods, which accelerate microbial production rates (Jin et al., 2022; Sadanaga et al., 2003). The close alignment between monthly NO_2 flux magnitudes and CO_2 trends at this site (Räsänen et al., 2017) confirms that nitrogen exchange is an intrinsic function of the ecosystem's phenological pulse. Notably, these observations of high summer NO_2 flux (Figure 7) agree with flux measurements reported from China (S. Chen et al., 2023), North America (Farmer and Cohen, 2008) and Europe (Brümmer et al., 2013), and are consistent with the high summer flux trend infered from satellite based modelling (van der A et al., 2008).

This phenological response is physically substantiated by the site's soil heat flux and soil temperature (5cm) profiles. Elevated summer thermal loading within the soil reduces the kinetic resistance to biogenic production, as microbial metabolic rates typically follow an exponential increase with temperature (Q_{10} sensitivity) until an optimal threshold is reached (Butterbach-Bahl et al., 2013). High daytime soil heat flux values, representing intense energy storage and conduction, facilitate the thermal venting of NO_2 from soil pores. This process occurs as a steepening temperature gradient between the subsurface and atmosphere drives the physical expansion and advective expulsion of soil-trapped gases (Schaufler et al., 2010). Concurrently, the sensible heat flux facilitates the convective energy necessary for vertical transport. As the surface warms, heat is transferred to the air via conduction and subsequently lofted through buoyant convection, allowing NO_2 pulses to overcome surface boundary layer resistance (Stull, 2012). Conversely, the winter transition to a deposition-heavy state aligns with a collapse of these fluxes. Declines in ambient temperature and relative humidity signal biological dormancy and a reduced evapotranspiration (Schaufler et al., 2010). During this period, the atmosphere becomes more stable, leading to a significant rise in aerodynamic resistance, which traps pollutants and promotes surface deposition (Wesely, 1989).

As the system moves through autumn (Figure 7), the frequency of positive fluxes decreased to 68.2%, accompanied by a significant decrease in the mean flux magnitude (0.0036 $\mu g\, m^{-2}\, s^{-1}$). This seasonal transition correlates with this reduction in soil and atmospheric moisture, weaker vertical mixing, and lower photosynthetic activity. As expected, flux magnitudes continued to decline through winter and spring, where positive fluxes accounted for only 65.0% and 67.4% of measurements and the mean fluxes remained fairly stable (between 0.0015-0.0024 $\mu g\, m^{-2}\, s^{-1}$). While these dry seasons are marked by high ambient NO_2 concentrations and prolonged surface stability, the overall biomass and surface drying have a dominating effect on deposition potential through increased surface resistance (Mariraj Mohan, 2016; Wesely and Hicks, 2000).

https://doi.org/10.5194/egusphere-2026-3066
Preprint. Discussion started: 11 June 2026

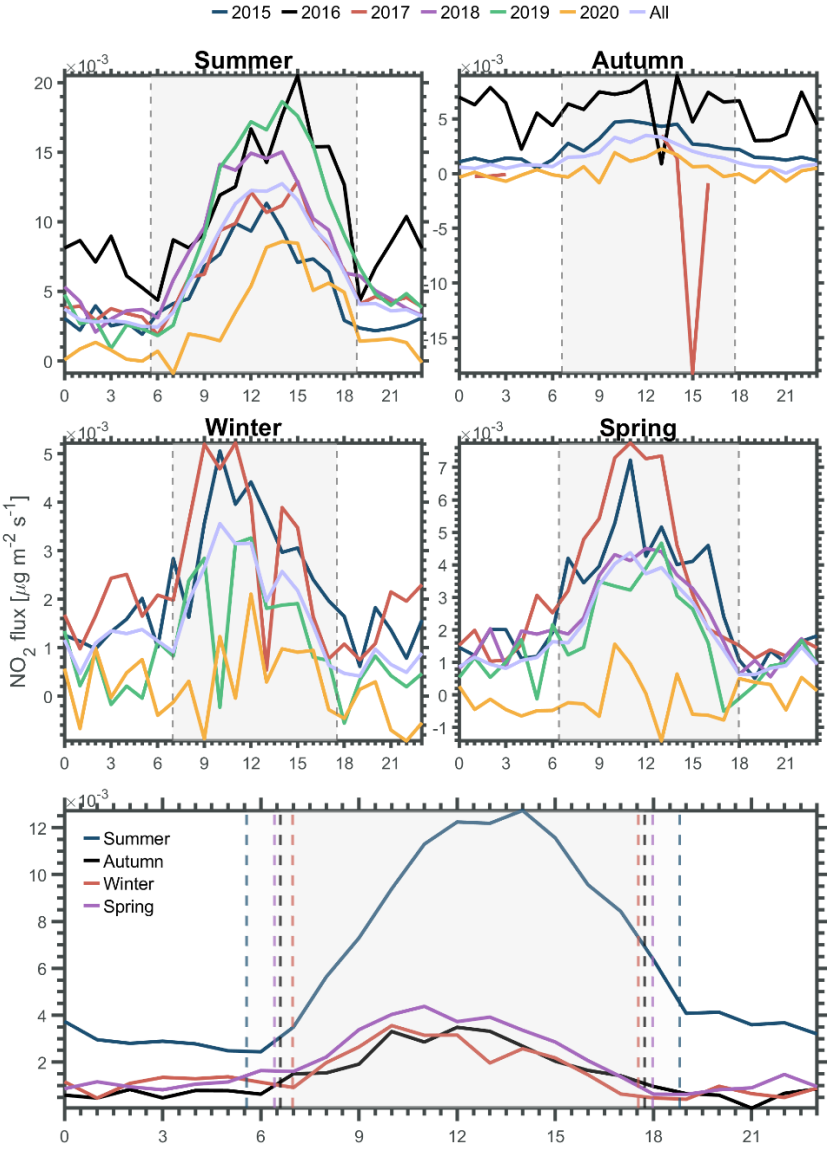

Figure 7: Seasonal diurnal variability of NO_2 emission flux measured at the Welgegund measurement site from March 2015 to September 2020. Upper panels show median hourly NO_2 fluxes (μg m^{-2} s^{-1}) for summer, autumn, winter, and spring, with coloured lines representing individual years (2015-2020) to illustrate interannual variability in amplitude and timing of exchange. The lower panel presents the aggregated median seasonal diurnal profiles calculated from all available years, highlighting systematic differences in flux magnitude between seasons. Vertical dashed lines indicate dynamically calculated seasonal sunrise and sunset times based on site latitude, longitude, and elevation, delineating daytime and nighttime periods.

https://doi.org/10.5194/egusphere-2026-3066
Preprint. Discussion started: 11 June 2026

To further evaluate the robustness of these patterns, a month-to-month intra-annual diurnal analysis was performed (Figure 8). These monthly panels demonstrate distinct intra-seasonal variability, highlighting subtle yet consistent changes in NO_2 flux behaviour while revealing additional structure regarding the timing and intensity of daily flux peaks and troughs. The diurnal NO_2 flux pattern displayed apparent seasonal variations, characterised by a significant midday upward flux from late spring to early autumn that corresponds with heightened solar radiation and increased boundary-layer turbulence. Between 08:00 and 14:00 local time, mean NO_2 fluxes remained consistently positive during summer months, peaking between 11:00 and 13:00 in a recurring midday enhancement, which is consistent with previously reported observations (Hanson et al., 1989; Pilegaard et al., 1998). This summer emission profile is physically substantiated by the site's soil temperature (5 cm) and soil heat flux profiles and elevated thermal loading reduces the kinetic resistance to biogenic production via a Q_{10} temperature sensitivity (Butterbach-Bahl et al., 2013). High daytime soil heat flux values facilitate the thermal venting of NO_2 from soil pores. As the temperature gradient between the subsurface and atmosphere steepens, the resulting physical expansion of pore air drives advective pulses of NO_2 into the surface layer.

This thermal expulsion is frequently amplified by rain-driven surface NO_x re-emissions, or "pulsing" events. In savanna-grassland systems, the first rainfall following a dry period triggers a rapid microbial metabolic response, often referred to as the Birch effect, where the sudden increase in soil moisture mineralises accumulated nitrogen, resulting in massive, short-lived NO_2 fluxes (Ganzeveld et al., 2002; Butterbach-Bahl et al., 2013). These moisture-triggered pulses are subsequently lofted into the atmosphere by the sensible heat flux, which generates the convective buoyancy required to overcome the quasi-laminar boundary layer (Stull, 1988). However, the abrupt daytime reversals and significant pre-dawn minima observed, even in summer, highlight a multi-factor interaction between surface resistance, radiation-driven mixing, and the entrainment of NO_2-rich air from higher altitudes during convective growth (Fowler, Cape and Unsworth, 1989). As the convective boundary layer deepens, it may entrain aloft industrial plumes, momentarily overriding local biogenic signals and contributing to the complex diurnal structures observed.

On the other hand, the transition into winter months marks a shift toward lower fluxes and frequent negative values, especially during nighttime and early morning hours (20:00-06:00). The lowest hourly mean flux, measured in July at 21:00 (-0.072 µg m^{-2} s^{-1}), which is an indication of deposition under stable nocturnal conditions, likely influenced by stomatal or cuticular uptake (Eugster and Hesterberg, 1996). Further evidence for active nighttime deposition was observed in February (Figure 8) and during other summer months, where significant pre-dawn minima indicated residual atmospheric NO_2 removal during times of restricted mixing. The contribution of stomatal processes to these deposition signals is evident; however, the considerable magnitude and frequency of nocturnal drops, coupled with abrupt daytime reversals, highlight the interaction of various factors: surface resistance, radiation-driven mixing, and the entrainment of elevated NO_2 from higher altitudes during convective growth (Fowler et al., 1989).

https://doi.org/10.5194/egusphere-2026-3066
Preprint. Discussion started: 11 June 2026

These temporally resolved features enhance the reliability of seasonal trends and underscore the need to elucidate diurnal flux structures to comprehend surface-atmosphere exchange dynamics in savannah-grassland systems. Overall, the net flux seasonality at this site appears to be driven by a complex interplay among emission intensity, boundary layer dynamics, and surface deposition efficiency. The high frequency and magnitude of upward fluxes in summer are likely enhanced by rain-driven surface NO_x re-emissions, high-temperature-promoted biogenic processes, and the entrainment of aloft industrial plumes into the surface layer. Conversely, during the winter season, the prevalence of deposition suggests an increased role of surface sink processes, characterised by lower boundary layer heights and reduced convective overturning. The overall diurnal structure of net NO_2 flux shows a similar pattern to other NO_2 flux observations (Behera and Sharma, 2011; Farmer et al., 2006; Geddes and Murphy, 2014; Karl et al., 2017; Min et al., 2014; Okamura et al., 2024; Stella et al., 2013) as well as observations of total reactive nitrogen (Ammann et al., 2012; Brümmer et al., 2013). These trends align well with CO_2 flux trends observed at the site (Räsänen et al., 2017), suggesting a strong linkage between NO_2 flux and phenological responses, or at least a strong response to the meteorological variables that drive these phenological responses. This linkage resonates further at the savanna ecosystem level, with other South African flux observations in the North-East (Archibald et al., 2009) and the more arid reaches of the biome to the South of the site (Maluleke, 2024; Maluleke et al., 2025). Interannual variability of NO_2 flux observed at the site showed similarities with NEE trends observed at Skukuza, where increased rainfall was associated with lower NEE flux magnitudes (Archibald et al., 2009).

https://doi.org/10.5194/egusphere-2026-3066
Preprint. Discussion started: 11 June 2026

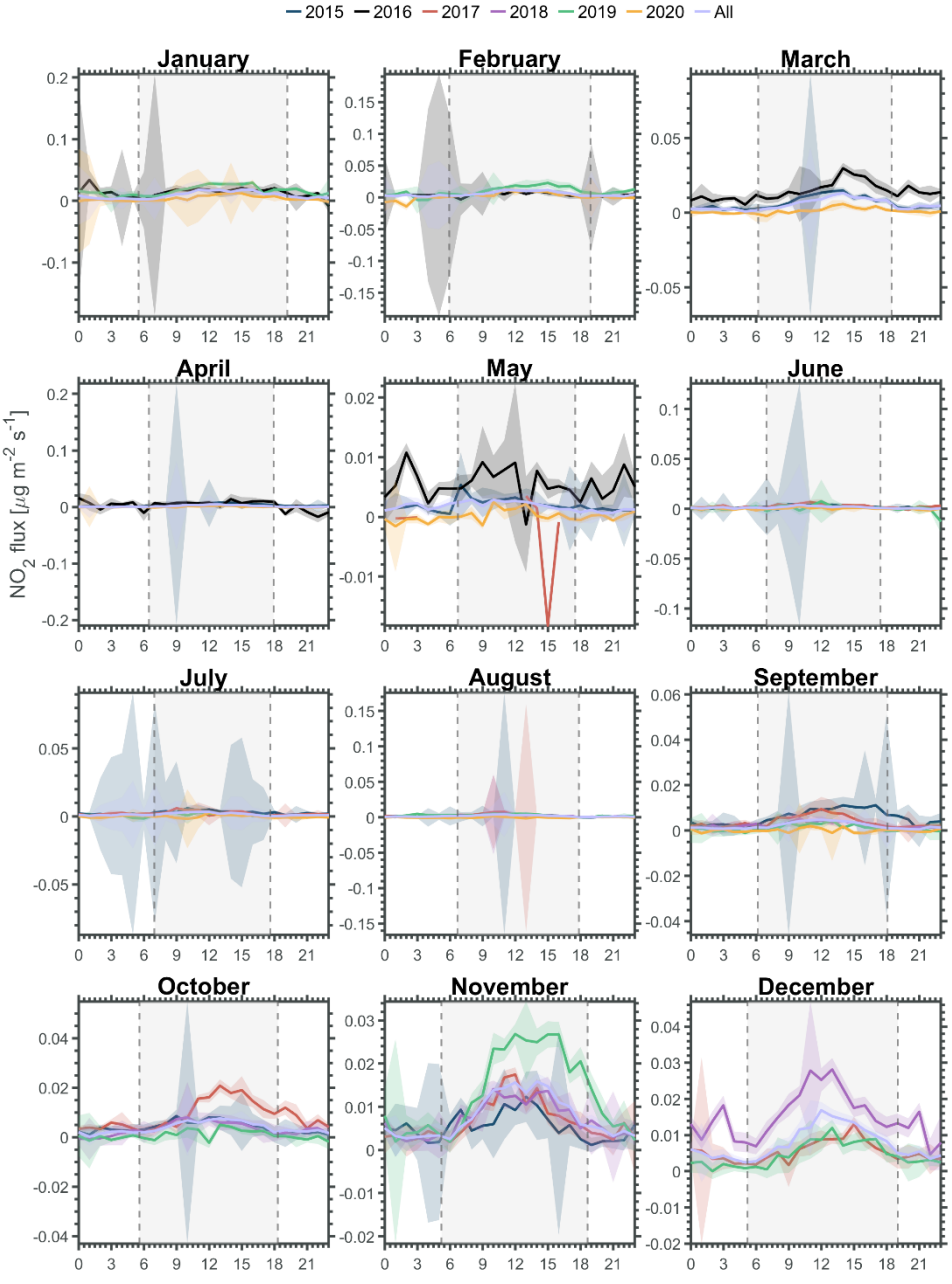

Figure 8: Month-by-month diurnal variation of NO_2 fluxes (μg m^{-2} s^{-1}) at the Welgegund measurement site from March 2015 to September 2020. Panels show median hourly NO_2 flux for each calendar month, with coloured lines representing individual years (2015–2020) and shaded envelopes indicating the interquartile ranges. Vertical dashed lines denote dynamically calculated monthly sunrise and sunset times, separating daytime and nocturnal exchange periods.

https://doi.org/10.5194/egusphere-2026-3066
Preprint. Discussion started: 11 June 2026

3.2.2 Partitioned NO_2 fluxes: emission vs deposition

To gain deeper insight into the bidirectional exchange of NO_2, fluxes were partitioned into their positive and negative components, using vertical direction to represent surface emission and deposition, respectively (Figure 9). This distinction isolates the underlying dynamics associated with each exchange direction and depicts unique temporal trends attributed to different mechanisms at the site.

A total of 15788 positive NO_2 flux observations were measured, with values ranging from near-zero to 5.58 $\mu g\, m^{-2}\, s^{-1}$. The distribution was positively skewed, with a mean of 0.0129 $\mu g\, m^{-2}\, s^{-1}$ and a median of 0.0055 $\mu g\, m^{-2}\, s^{-1}$ (IQR = 0.0096 $\mu g\, m^{-2}\, s^{-1}$). Emission fluxes showed a marked seasonal signal: during the wet summer season (October-March), the average emission rate (mean = 0.0161 $\mu g\, m^{-2}\, s^{-1}$; median = 0.0083 $\mu g\, m^{-2}\, s^{-1}$) was nearly double that of the dry season (April-September; mean = 0.0086 $\mu g\, m^{-2}\, s^{-1}$; median = 0.0033 $\mu g\, m^{-2}\, s^{-1}$). Interquartile ranges mirrored this trend, highlighting enhanced variability in emission processes during the wetter, warmer months, consistent with temperature- and moisture-driven microbial NO_x production from soils (Feig et al., 2008; Jin et al., 2022; Stewart et al., 2008)

Interannual patterns in positive NO_2 flux further underscore variability within the wet summer season. The years 2015 and 2016 exhibited the highest mean positive fluxes (0.0157 and 0.0249 $\mu g\, m^{-2}\, s^{-1}$, respectively), alongside elevated medians and interquartile ranges (IQRs). In contrast, 2020 recorded the lowest annual mean (0.0073 $\mu g\, m^{-2}\, s^{-1}$), with the lowest median observed across several months (e.g., April-September), likely due to incomplete flux measurements for the year, as data collection was limited to half of the summer. Monthly medians peaked in summer months such as December 2018 (0.0178 $\mu g\, m^{-2}\, s^{-1}$) and January 2019 (0.0177 $\mu g\, m^{-2}\, s^{-1}$), coinciding with both the highest IQRs and mean values indicative of dynamic surface emission regimes likely modulated by soil moisture pulses and plant canopy interactions (Chaparro-Suarez et al., 2011a; ELLER and SPARKS, 2006).

In contrast, negative fluxes of NO_2, representing contributions towards surface deposition, were recorded 5893 times with values ranging from -4.23 to nearly zero. The dataset was negatively skewed (mean = -0.0131 $\mu g\, m^{-2}\, s^{-1}$; median = -0.0024 $\mu g\, m^{-2}\, s^{-1}$), with a broader spread during the wet summer season (IQR = 0.0082 $\mu g\, m^{-2}\, s^{-1}$) compared to the dry season (IQR = 0.0036 $\mu g\, m^{-2}\, s^{-1}$). Although deposition flux was generally weaker in magnitude than emission, interannual patterns suggest specific periods where surface uptake dominated. For instance, 2016 exhibited the strongest mean deposition flux (-0.0366 $\mu g\, m^{-2}\, s^{-1}$) and the highest interquartile range (IQR = 0.017 $\mu g\, m^{-2}\, s^{-1}$), indicating a year of enhanced deposition potential. This was likely tied to increased surface wetness during the transition from summer to autumn (March-May), where pre-dawn air temperatures decline, resulting in dew formation (Baier, 1966), coupled with maximum diurnal concentrations.

Extreme flux events, defined as those exceeding the 99th percentile threshold (0.0662 $\mu g\, m^{-2}\, s^{-1}$), occurred 217 times. Of the extreme positive fluxes, 28.5% (N = 62) occurred in 2015, with the most extreme positive flux recorded on 8 April 2015 (5.58 $\mu g\, m^{-2}\, s^{-1}$). These high-flux emission events are characteristic of short-lived microbial flushes or anthropogenic plumes, which coincide with favourable dispersion and boundary layer conditions. Similarly, 217 extreme negative fluxes fell below the 1st

https://doi.org/10.5194/egusphere-2026-3066
Preprint. Discussion started: 11 June 2026

percentile threshold (-0.0439 μg m^{-2} s^{-1}), with 2015 accounting for the most significant magnitudes and representing 35.5% (N = 77) of deposition flux extremes. The lowest flux observed was -4.23 μg m^{-2} s^{-1}, measured on 12 August 2015. High-magnitude extreme flux events were episodic and did not correspond well with periods of high ambient NO_2 concentrations. Additionally, no clear trends were observed in either annually or monthly grouped extreme events. However, this may reflect another underlying meteorological driver, such as isolated surface events influencing extreme flux intensities.

3.3. NO_2 deposition velocity dynamics

The surface-atmosphere exchange of NO_2 flux at this site reflects a system that predominantly acts as a source but exhibits strong bidirectional behaviour modulated by seasonal meteorological cycles, phenological changes in vegetation, and soil moisture dynamics. The contrasting magnitudes, distributions, and extremes of positive and negative NO_2 flux highlight the need to consider both components independently when quantifying net atmospheric exchange and modelling regional NO_2 contributions to nitrogen budgets. The half-hourly NO_2 v_d were calculated from all downward-directed fluxes (N = 5893) (Figure 9) and reflected both stable background exchange processes and episodic high-intensity events. The distribution was highly right-skewed with a mean of 1.488 cm s^{-1}, a median of 0.271 cm s^{-1}, and an IQR of 0.480 cm s^{-1}. The observed skewness in NO_2 v_d is characteristic of dry deposition datasets (e.g., Hanson et al., 1990; Massad et al., 2010), where turbulence and surface resistance modulate fluxes in a nonlinear manner, highlighting the importance of utilising non-parametric statistics (e.g., medians and IQRs) for a more reliable interpretation.

As depicted in Figure 9, during the study period, the NO_2 v_d exhibited recurring monthly patterns, with relatively consistent median values throughout the year, ranging from 0.231 cm s^{-1} (April) to 0.355 cm s^{-1} (May). In the absence of high-magnitude outliers (e.g., above the 90th percentile, v_d > 0.285 cm s^{-1}), the monthly means converge closer to 0.1-0.12 cm s^{-1}, well within the expected range for vegetated grasslands (Zhang et al., 2003). However, when extreme values are retained, monthly means in 11 of 12 months exceed the modelled maximum v_d for NO_2 (Zhang et al., 2003). However, the data collection from May 2017 is represented by very few flux observations (N = 12) and is likely not an accurate representation of the month. The spike in v_d patterns in May suggest that increased surface wetness, resulting from dew (Baier, 1966), linked to seasonal transitions, may enhance deposition pathways (Eugster and Hesterberg, 1996; Zhang et al., 2005).

https://doi.org/10.5194/egusphere-2026-3066
Preprint. Discussion started: 11 June 2026

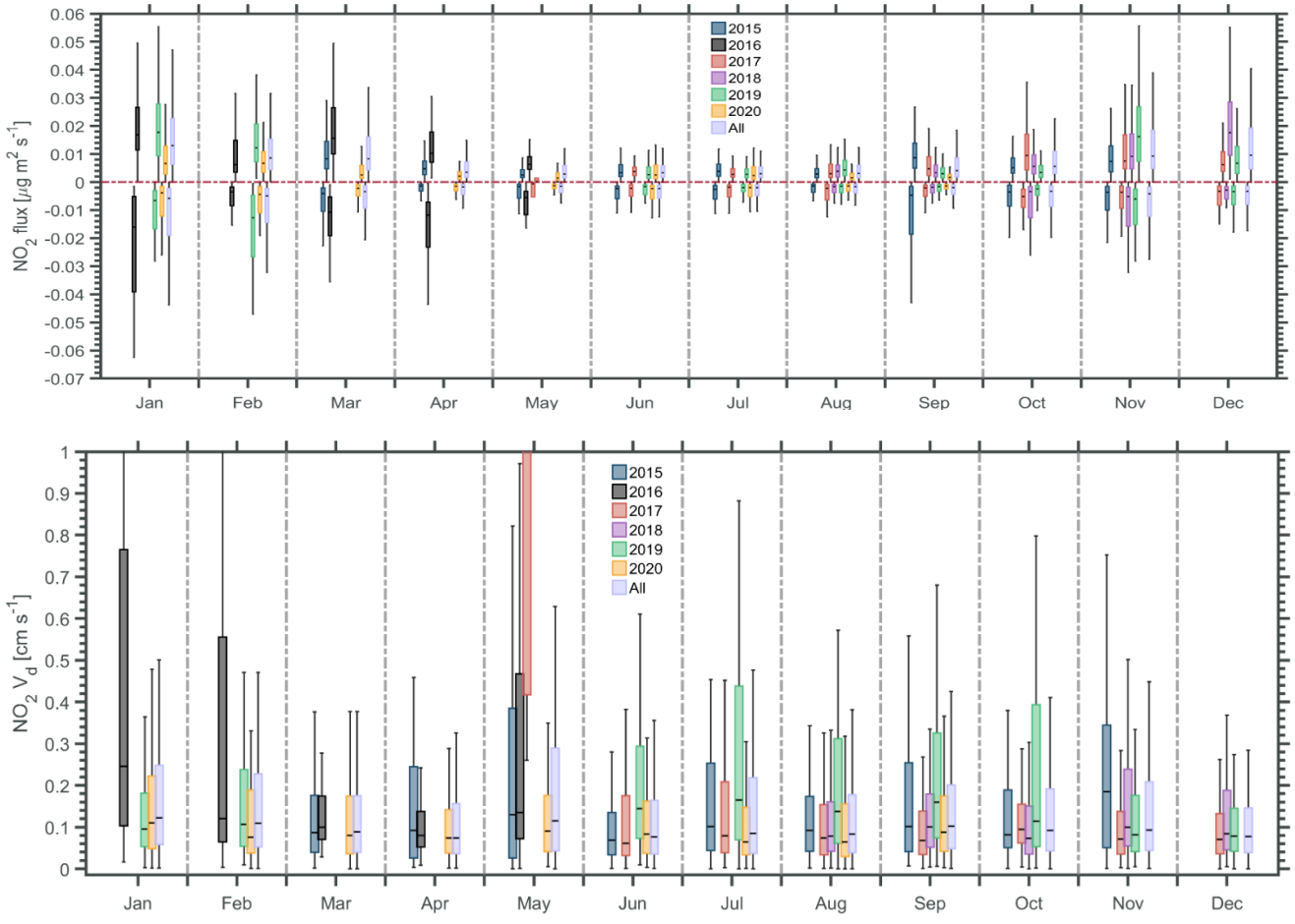

Figure 9: Monthly distributions of partitioned NO_2 fluxes (µg m^{-2} s^{-1}) and deposition velocity (v_d, cm s^{-1}) at the Welgegund measurement site from March 2015 to September 2020. Box-and-whisker plots show the statistical distribution of positive (emission) and negative (deposition) flux components, with boxes representing the interquartile range (25th - 75th percentiles), the red line indicating the median, and whiskers extending to 1.5 × IQR. Colours distinguish individual years, while the aggregated "All" category represents the combined dataset across all years, illustrating both seasonal variability and interannual differences in emission and deposition behaviour.

Interannual variability was apparent within the observation period, where medians for 2015 and 2016 were only 0.29 and 0.38 cm s^{-1}, but their distributions were strongly right-skewed by many high magnitude v_d observations. The annual means of these years were 2.90 and 3.89 cm s^{-1}, which are well above the modelled maximum v_d values for NO_2 (1.4-1.6 cm s^{-1}) proposed by Zhang, Brook and Vet (2003) for all land cover classifications. Although, the annual averages of 2015 and 2016 are similar to inferential model means for wet savannas in Western and Central Africa (Adon et al., 2013). In contrast, annual mean v_d values for 2017 to 2020 ranged from 0.82 to 1.52 cm s^{-1}, aligning more closely with daily v_d maxima observed from a tropical pasture site (Trebs et al., 2006) as well as inferential modelled estimates from various South African sites (Mompati et al., 2019).

https://doi.org/10.5194/egusphere-2026-3066
Preprint. Discussion started: 11 June 2026

However, annual medians indicated that 2016 (0.38 cm s^{-1}) and 2019 (0.16 cm s^{-1}) were significantly different ($p < 0.05$) and represent consistently stronger deposition. Median v_d observed for other years within the observation period had lower magnitudes, ranging between 0.24 cm s^{-1} and 0.28 cm s^{-1}.

At the seasonal scale, v_d values were relatively stable, although subtle contrasts were evident. The wet season (October-March) had a slightly higher mean (0.77 cm s^{-1}) and IQR (0.21 cm s^{-1}) compared to the dry season (April-September), which recorded a mean of 0.62 cm s^{-1} and IQR of 0.22 cm s^{-1}. The differences between seasons were not statistically significant ($p < 0.05$), which conflicts with seasonal trends reported from inferentially modelled findings. The overall v_d observed at WAMS were at least twice the magnitude of seasonal inferentially modelled estimates reported by Mphepya (2002) (0.04-0.28 cm s^{-1}) and Josipovic *et al.* (2011) (0.04-0.26 cm s^{-1}), which informs on the more polluted Highveld region.

Monthly v_d distributions supported the observed seasonal stability, with similar interquartile ranges across most months (Figure 12). Monthly mean and median trends differed substantially within the study period: medians gradually declined from January (0.35 cm s^{-1}) to April (0.23 cm s^{-1}), followed by a spike in May (0.36 cm s^{-1}). Widespread meteorological shifts, such as increased dew formation (Muselli and Beysens, 2021) and prolonged atmospheric stability during the early dry season (Gierens et al., 2019) can enhance surface uptake efficiency. The observed May spike in median V_d coincides with declines in planetary boundary layer height (Korhonen et al., 2014), by June the minimum height is frequently <300m (De Lange et al., 2021). In addition to the stability of inversion layers, local studies have indicated a high frequency of dew events (Baier, 1966), most notably in the presence of biocrusts (Li et al., 2021), for which the southern African region is in abundance of (Rodriguez-Caballero et al., 2018).

The v_d pattern is very different for monthly means, which had an overall decline from January (2.09 cm s^{-1}) onwards, but peaked in November (3.59 cm s^{-1}). Interestingly, the months with the lowest mean v_d occurred consecutively as August (0.92 cm s^{-1}), September (1.06 cm s^{-1}) and October (0.86 cm s^{-1}). These months of consecutively low mean v_d coincide with noticeable increases in NEE (Räsänen et al., 2017), CO (Laban et al., 2018), O_3 (Donnou et al., 2024) and variability of VOCs (Jaars et al., 2014) at the site. These factors combined support the potential for local peroxy radicals to drive a net O_3 production. The observed monthly v_d contrasts distinctly with inferential model outputs from other equatorial African regions which ranged from 0.12 to 0.38 cm s^{-1} (Adon et al., 2013). However, the local concentrations at those sites (0.5-4.5 ppb) are not substantially different from the mean diurnal concentrations (0.8 - 4.9 ppb) observed during the study period. This suggests that observed V_d medians are most comparable to inferential models, as the mean v_d is greatly influenced by extreme events.

Diurnal patterns in v_d were described as hourly box and whisker plots representing the entire study period (Figure 10). Each hourly bin consisted of 174 to 320 half-hourly measurements, with >200 hourly measurements for all but 3 bins (13.00-15.00). Hourly v_d observations had a distinct diurnal pattern with increased v_d during daylight hours and lower v_d magnitudes observed overnight. This generalized diurnal trend is replicated in multiple inferential models (Mphepya, 2002; Zhang et al., 2003, 2002). Daytime v_d had a mean of 2.11 cm s^{-1} and a median of 0.44 cm s^{-1}, with an IQR of 0.75 cm s^{-1}. While nighttime v_d was

https://doi.org/10.5194/egusphere-2026-3066
Preprint. Discussion started: 11 June 2026

approximately half these magnitudes, with a mean of 1.20 cm s^{-1}, a median of 0.22 cm s^{-1} and an IQR of 0.32 cm s^{-1}. Hourly binned v_d had similar medians within the daytime and nighttime groups, but means were highly variable. The hours with the greatest v_d were 01.00 (mean=5.87 cm s^{-1} and median= 0.20cm s^{-1}), 13.00 (mean= 3.92 cm s^{-1} and median= 0.45cm s^{-1}), 10.00 (mean= 3.89cm s^{-1} and median= 0.49cm s^{-1}) and 15.00 (mean= 3.42 cm s^{-1} and median= 0.53cm s^{-1}). However, the high mean observation noted at 01.00 could likely be an instrumental artefact driven bythe two highest v_d observations from the entire timeseries. The hours with the lowest v_d were 03.00 (mean=0.35 cm s^{-1} and median= 0.20cm s^{-1}), 22.00 (mean= 0.37cm s^{-1} and median= 0.23 cm s^{-1}) and 02.00 (mean= 0.39 cm s^{-1} and median= 0.19cm s^{-1}).

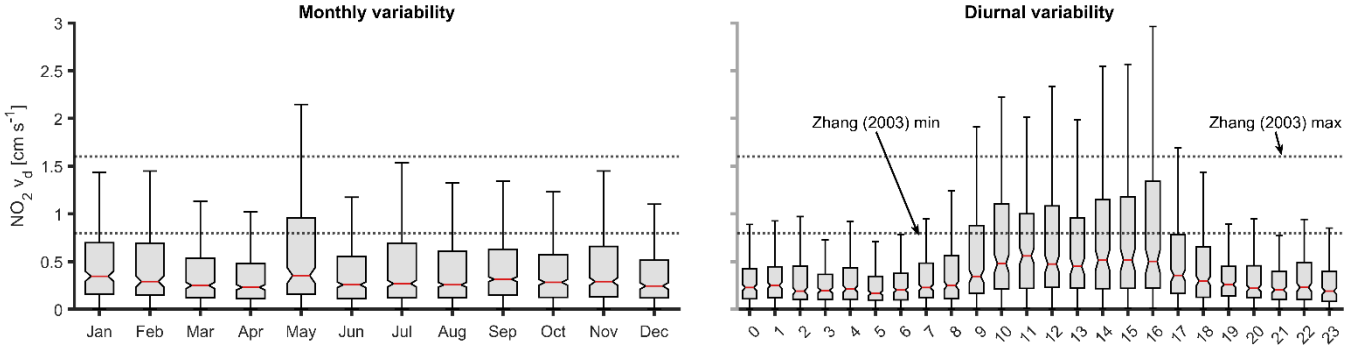

Figure 10: Distribution of measured NO_2 v_d presented as box-and-whisker plots illustrating seasonal (monthly; left) and diurnal (hourly; right) variability at the savanna measurement site. Boxes denote the interquartile range (25th - 75th percentiles), the central red line indicates the median, and whiskers extend to 1.5×IQR; outliers are omitted for clarity to emphasise central tendencies in surface–atmosphere exchange. The pronounced daytime enhancement in NO_2 v_d and reduced nocturnal values reflect the strong coupling between stomatal activity, canopy turbulence, and aerodynamic transport, highlighting the role of canopy and surface resistances in regulating reactive nitrogen uptake. Horizontal dotted lines indicate the upper range of NO_2 v_d predicted for various LUCs (0.8-1-6cm s^{-1}) by the inferential resistance parameterisation of Zhang, Brook and Vet (2003), providing a literature-based benchmark for evaluating observed deposition efficiencies.

3.4. Compensation point

To investigate the compensation point (C_P) at the ecosystem level, we consider the median NO_2 flux at 1 ppb bin width in Figure 11. Given the strong seasonality in ecosystem NO_2 flux, Figure 11 is plotted for both dry and wet season. Only daytime data with PAR radiation > 100 µmol m^{-2} s^{-1} and wind speed > 1.5 m/s were included. Furthermore, precipitation and fog are excluded by selecting RH < 85%. Periods of extreme heat/dryness are excluded by limiting estimated VPD < 3.0 kPa; VPD was estimated using Tetens equation based on T and RH. The zero-intercept of linear regression to the data in Figure 11 indicates ecosystem-scale C_P of 6.60 ppb (4.60-14.64 ppb) for the dry season and C_P of 6.66 ppb (5.37-15.96 ppb) for the wet season, respectively.

https://doi.org/10.5194/egusphere-2026-3066
Preprint. Discussion started: 11 June 2026

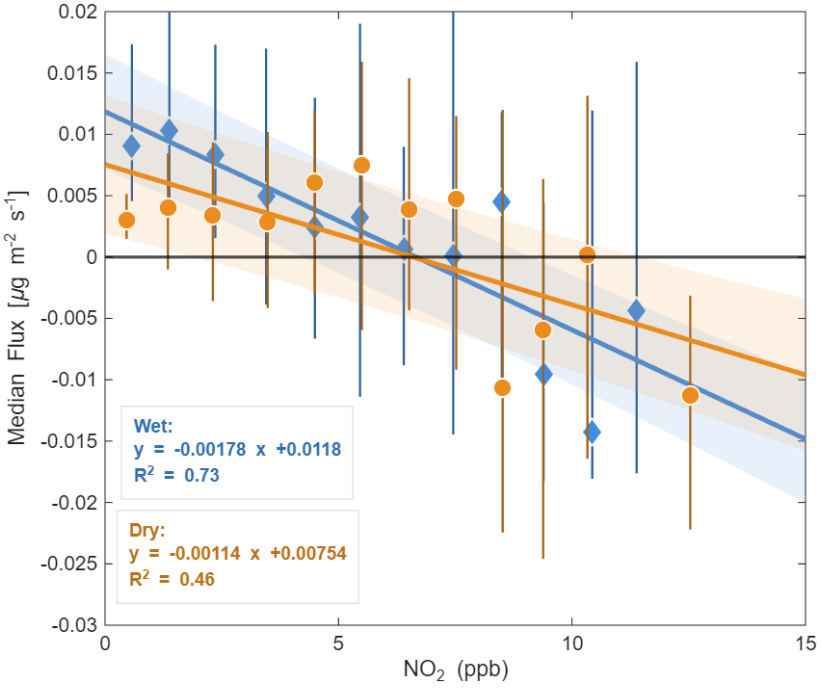

Figure 11. Median daytime NO_2 flux at 1 ppb bin width. Error bars indicate 25th and 75th percentile. Only bins with at least 10 30-minute flux observations are included.

The C_P values that we observe are higher than what have been previously reported for tropical, subtropical and temperate forest tree species, where the observations range from 0 to 3 ppb for NO_2 (Ke et al., 2025). However, the previous flux observations linked to C_P are limited to chamber studies of leaf- or branch-level measurements (Breuninger et al., 2013; Conrad, 1994) and thus exclude soil dynamics. Since soil is often a source of NO and NO_2 (Butterbach-Bahl et al., 2013; Feig et al., 2008), it is to be expected that the ecosystem scale compensation point observed here is higher than at the leaf level.

Using Eq. 1 and the linear fits in Figure 11, we can estimate the NO_2 dry deposition velocity. For the dry season, we obtain v_d of 0.061 cm s^{-1}, while for the wet season, aslightly higher v_d of 0.095 cm s^{-1}. We attribute the higher wet season v_d to increased LAI and NDVI (Räsänen et al., 2017); that provide increased surface for deposition. These v_d estimates are similar, although less than the seasonal averages previously derived from inferential techniques: 0.04-0.26 cm s^{-1} (Mphepya, 2002) and 0.05-0.15 cm s^{-1} (Phala, 2015). This is likely due to WAMS being a regional background site, while the observations of Mphepya (2002) and Phala (2015) were in closer proximity to high-emission areas. These observations are within the same order of magnitude as v_d parameterizations from Zhang, Brook and Vet (2003). It is important to note that our v_d estimates are limited to median flux conditions and does not account for the occurrence of high magnitude events that would be associated with greater v_d potential or nighttime conditions that are commonly impacted by low turbulence.

https://doi.org/10.5194/egusphere-2026-3066
Preprint. Discussion started: 11 June 2026

3.5. Comparison of observed and modelled deposition velocities

The eddy-covariance measurements presented here constitute the first micrometeorological constraints on NO_2 v_d for the African continent, providing a rare opportunity to directly evaluate inferential deposition schemes that have historically relied on parameterisations developed outside semi-arid savanna systems. Observed v_d values were compared with 3-hourly estimates derived from a modified Zhang et al. (2003) "big-leaf" inferential model (Figure 12). Because the model framework does not explicitly represent episodic high-magnitude deposition events, comparisons were restricted to observations below the 90th percentile to ensure consistency in the evaluation.

Modelled NO_2 v_d exhibited comparatively low variability (mean = 0.209 cm s^{-1}; median = 0.155 cm s^{-1}) relative to the broader and strongly skewed observational distribution (Sect. 3.3.3), highlighting fundamental differences in the representation of exchange processes. A paired t-test confirmed a significant mismatch between modelled and measured deposition velocities ($t = 5.36$, $p < 0.01$, $df = 323$). Annual and monthly diurnal comparisons (Figure 12) revealed systematic biases: the inferential model consistently overestimated daytime deposition while slightly underestimating nocturnal exchange. This resulted in an overall positive mean bias (MB = 0.0382 cm s^{-1}), driven primarily by daylight discrepancies (MB_{Day} = 0.0631 cm s^{-1}), whereas nighttime bias was negligible ($MB_{Night} \approx 8.7 \times 10^{-5}$ cm s^{-1}).

The magnitude and structure of these biases varied across years, suggesting that key controls on NO_2 deposition, such as soil moisture pulses, canopy dynamics, and turbulence regimes, are not fully resolved by the parameterisations or by remotely sensed inputs used in the inferential approach. Seasonal contrasts further emphasised these limitations: model performance was strongest during winter (MB_Winter = 0.00308 cm s^{-1}), when atmospheric conditions are relatively stable, but deteriorated during the wet summer season (MB_Summer = 0.0537 cm s^{-1}), when biological and meteorological drivers of exchange intensify. Notably, the onset of simulated daytime increases in V_d lagged observations by approximately three hours, pointing to a misrepresentation of boundary-layer development and vegetation–atmosphere coupling within the model framework. At the monthly scale, the divergence between modelled and observed diurnal cycles became more pronounced, despite both datasets reproducing the broad wet–dry seasonal contrast (Figure 12). These findings indicate that widely used inferential models capture first-order seasonal tendencies but fail to reproduce the magnitude, timing, and variability of NO_2 deposition under semi-arid savanna conditions.

The implications extend beyond this site: systematic daytime overestimation suggests that regional and continental-scale NO_2 dry-deposition budgets for Africa may currently be biased high, particularly where parameterisations derived from temperate ecosystems are applied without regional calibration. These first direct flux measurements from an African savanna challenge prevailing assumptions embedded in inferential deposition schemes, demonstrating that global nitrogen deposition budgets may be systematically biased where parameterisations are extrapolated beyond the ecosystems in which they were developed. Considering that some remotely sensed datasets have a limited observation period over South Africa, such as TROPOMI overpasses at ~13.30 (Kai-Sikhakhane et al., 2024), the overestimations of the commonly used 'Big-leaf' inferential model would likely lead to significant overestimation of NO_2 dry deposition in the South African region. Furthermore, the disconnect

https://doi.org/10.5194/egusphere-2026-3066
Preprint. Discussion started: 11 June 2026

between the model and observations regarding the timing of diurnal increases in NO_2 v_d suggests that local meteorology and vegetation dynamics may have a significant impact on mediating v_d.

595

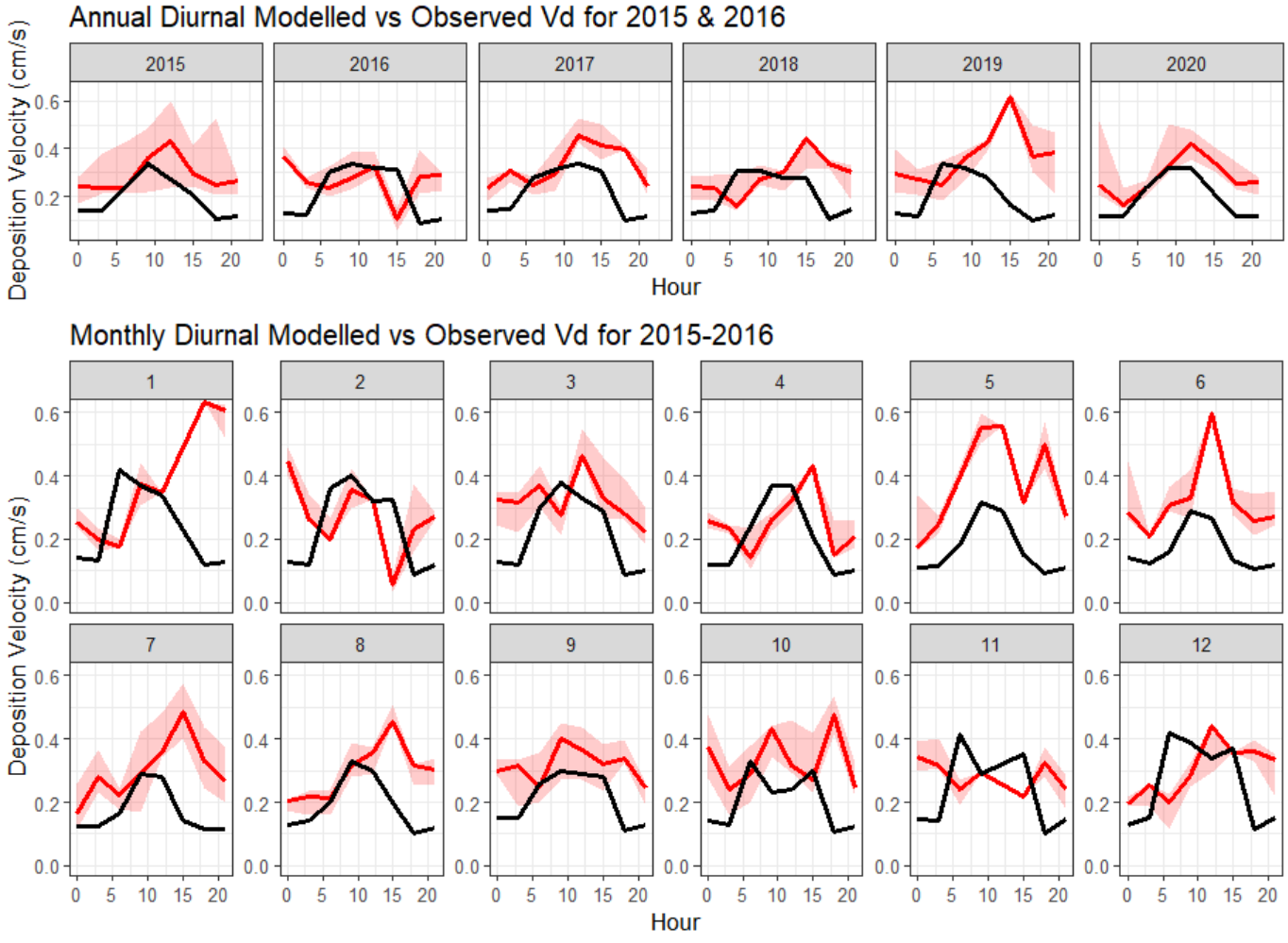

Figure 12: Comparison of annual (top) and monthly (bottom) 3-hour median V_d observations (red line) at Welgegund, South Africa and inferential model outputs (black line). Interquartile range (25th to 75th percentiles) for 3-hourly V_d observations are provided as red shaded area.

https://doi.org/10.5194/egusphere-2026-3066
Preprint. Discussion started: 11 June 2026

3.6. Synthesis and global context

The WAMS site represents the first in-situ observations of NO_2 fluxes in an African savanna ecosystem. The heterogeneous vegetation structure, with an open canopy and a mosaic of grassland and shrub vegetation, forces an enhanced level of sub-canopy turbulence with reduced woody respiration potential in comparison to forest ecosystems. This provides a contrasting structure to closed canopy forests that dominate as NO_2 sinks in the existing literature: temperate forests of Europe and North America (Geddes and Murphy, 2014; Horii, 2002; Zhang et al., 2005) and subtropical forests in China (Kang et al., 2023; Ke et al., 2020) that have strong within-canopy chemical change pathways (Farmer and Cohen, 2008; Min et al., 2014). Shorter vegetation types, are thought to be weaker NO_2 sinks owing to variable physiological responses and internal leaf resistance potentials (Stella et al., 2013; Zhang et al., 2003). This suggests that strictly considering vegetation structure, a savanna ecosystem is expected to have a reduced impact of in-canopy transformations and include contributions from shorter vegetation; to occur somewhere between these two LUCs.

The C_P observed at WAMS was higher than recent chamber flux observations from temperate forest trees that were unable to exclusively confirm C_P existence (Breuninger et al., 2013; Chaparro-Suarez et al., 2011a). Within literature the existence of NO_2 C_P is further debated; although plant physiological responses indicate potential flux contribution at the ecosystem level (Conrad, 1994; Thoene et al., 1996; Wang et al., 2020). In the context, of semi-arid ecosystems, drought tolerant species for which enhanced stomatal conductance is a well-known adaptation (Ali et al., 2020; Farquhar and Sharkey, 1982; Hossain et al., 2016) has been shown to enhance the uptake of NO_2 (Chaparro-Suarez et al., 2011a). While plants readily take up NO_2 through stomata for conversion into osmoregulation metabolites and stomata signalling chemicals (Feng et al., 2024; García-Mata and Lamattina, 2001), observations from (Guerrieri et al., 2010; Wang et al., 2016) indicated enhanced stomatal uptake in systems that are frequently exposed to moisture limitations.

These plant physiological features align well with the local context of the semi-arid grassland, savanna and agriculture systems surrounding WAMS and the ambient NO_2 concentrations of a background site downwind of a global NO_2 hotspot. Furthermore, similar conditions were simulated by Teklemariam and Sparks (2006) and Chaparro-Suarez, Meixner and Kesselmeier, (2011b) which observed foliar uptake of NO_2. However, available moisture plays a pivotal role in controlling biomass interactions in many African systems. This adds an additional layer of complexity by 'switching off' biomass in-canopy transformations during dry periods through physiological responses to water stress. While soil moisture declines and surface heating results in widespread venting of NO_2 from sub-surface stocks that are lofted by convective currents. Thus, in moisture-limited systems, soil fluxes dominate as the source of NO_2 driving an emissions-driven regime (Butterbach-Bahl et al., 2013; Delaria et al., 2018; Rummel et al., 2002; Schaufler et al., 2010). While the addition of moisture to the system facilitates an enhanced biological response that has been detected from great height (Harris et al., 1996) and in some subtropical forests (Kang et al., 2023), our observations show that the savanna surface-level emission conditions persist with sustained moisture inputs.

https://doi.org/10.5194/egusphere-2026-3066
Preprint. Discussion started: 11 June 2026

Although WAMS is considered a background site, it is influenced by upwind anthropogenic emissions that drive high ambient concentrations, resulting in substantial potential for dry deposition throughout the observational record. This was further reinforced by lower dry deposition ranges observed under C_P regression criteria which suggests that high magnitude events contribute substantially to the total system deposition. These high magnitude events likely account for the large proportion of observations that exceeded modelled expectations during daylight hours and during the transition from wet to dry season - when ambient temperatures and NDVI declined but rainfall and dew events persisted. The mismatches between the observations and modelled estimates imply several possibilities: model parameterizations are not calibrated for heterogeneous vegetation structures like savannas; local meteorology is ineffectively captured within the inferential model; or a chemical component has not been accounted for as a localised driver of ambient chemistry. This has significant implications for NO_2 flux and deposition estimations in uncharacterised landscapes, such as many sub-tropical systems where moisture limitation is a common seasonal and interannual effect. Furthermore, many semi-arid systems across Africa, South America and Australia exhibit ecosystem dynamics similar to those described here, highlighting considerable uncertainty in the contribution of semi-arid ecosystems to global Nitrogen budgets.

4. Conclusions

Herein, we present the first eddy covariance measurements of NO2 fluxes at a South African background site. Observations of net and partitioned fluxes of NO_2 indicated that the site is predominantly a source, with the majority of emissions occurring during daytime hours and prolific amplification of emission magnitudes during the summer rainfall season. Nighttime fluxes were smaller and likely mediated by pronounced atmospheric stability and reduced turbulent mixing, which persists during winter conditions to drive lower daytime flux magnitudes.

Deposition velocity had strong duality between day and nighttime hours, but insignificant seasonal trends. Thus, it is more likely that regional dry deposition, within the context of semi-arid landscapes, is governed by surface wetting as a result of condensation, dew and the onset of the wet season. The overall temporal trends in v_d were poorly reproduced by the inferential model, potentially due to mediation by local- to regional-scale environmental features, which may not be well-defined in the model. These discrepancies call attention to the need for more representative validation datasets to improve the accuracy of dry deposition estimation in different ecosystems. By acknowledging the land-atmosphere coupling of eddy covariance studies, we are able to improve understanding of mesoscale dry deposition dynamics, which act as a critical link between different scales of Earth observation.

An abundantly clear interannual variability persisted across all observations, which highlights the dynamic forcing of near-surface NO_2 at various timescales. Furthermore, the duration for which this study was observed also includes various environmental conditions, such as drought, which approximates regionally anticipated future climate conditions. These findings underscore the complexity of deposition dynamics within African landscapes, where further work is necessary to accurately predict future dry deposition under variable climates.

https://doi.org/10.5194/egusphere-2026-3066
Preprint. Discussion started: 11 June 2026

5. Data availability

The data of this paper are available upon request to Kerneels Jaars (kjaars@sun.ac.za) and Pieter van Zyl (pieter.vanzyl@nwu.ac.za).

6. Author contributions

TH conceptualised the study, performed the data curation, formal analysis, and investigation, developed the methodology, created all visualisations, and prepared the original manuscript draft. KJ and PGvZ supervised the study, contributed to its conceptualisation and design, and acquired funding. MJ and VV contributed to the installation of the QCL eddy covariance system, assisted with flux processing methodology, and contributed to data curation. MA contributed to the eddy covariance infrastructure and long-term operation at WAMS. MA developed and provided the inferential deposition model adapted for African ecosystems. JPB, GTF, MK, and LL contributed site resources, long-term ancillary measurement infrastructure, and the establishment and continued operation of the Welgegund Atmospheric Measurement Station. GTF and MJ further contributed to co-supervision of the study. All authors contributed to reviewing and editing the manuscript.

7. Competing interests

Kerneels Jaars is a member of the editorial board of Biogeosciences. The remaining authors declare that they have no competing interests.

8. Acknowledgements

This publication forms part of the output of the Biogeochemistry Research Infrastructure Platform (BIOGRIP) of the Department of Science and Innovation of South Africa, which supports the Welgegund station. The authors gratefully acknowledge the Welgegund Atmospheric Measurement Station (WAMS), jointly established and operated by the Atmospheric Chemistry Research Group at North-West University (NWU), Potchefstroom, South Africa, and the Finnish Meteorological Institute (FMI), Helsinki, Finland, as the primary research infrastructure for this study. The authors thank the owners and managers of Welgegund farm for continued site access and support. The authors wish to thank Diederik and Jackie Hattingh and their families, who own the commercial farm on which the Welgegund measurement station is situated. Tamryn Hamilton acknowledges NWU for postgraduate research support.

https://doi.org/10.5194/egusphere-2026-3066
Preprint. Discussion started: 11 June 2026

9. Financial support

The financial assistance of the NRF towards this research is hereby acknowledged (grant no. MND200520523132 & PMDS230502100985). Opinions expressed and conclusions arrived at are those of the authors and are not necessarily attributed to those of the NRF.

References

Adon, M., Galy-Lacaux, C., Delon, C., Yoboue, V., Solmon, F., Kaptue Tchuente, A.T., 2013. Dry deposition of nitrogen compounds (NO2, HNO3, NH3, sulfur dioxide and ozone in west and central African ecosystems using the inferential method. Atmospheric Chem. Phys. 13, 11351–11374. https://doi.org/10.5194/acp-13-11351-2013

Ahlström, A., Raupach, M.R., Schurgers, G., Smith, B., Arneth, A., Jung, M., Reichstein, M., Canadell, J.G., Friedlingstein, P., Jain, A.K., 2015. The dominant role of semi-arid ecosystems in the trend and variability of the land CO2 sink. Science 348, 895–899.

Ali, S., Hayat, K., Iqbal, A., Xie, L., 2020. Implications of Abscisic Acid in the Drought Stress Tolerance of Plants. Agronomy 10, 1323. https://doi.org/10.3390/agronomy10091323

Allan, R.P., Arias, P.A., Berger, S., Canadell, J.G., Cassou, C., Chen, D., Cherchi, A., Connors, S.L., Coppola, E., Cruz, F.A., 2023. Intergovernmental Panel on Climate Change (IPCC). Summary for Policymakers, in: Climate Change 2021: The Physical Science Basis. Contribution of Working Group I to the Sixth Assessment Report of the Intergovernmental Panel on Climate Change. Cambridge University Press, pp. 3–32.

Ammann, C., Wolff, V., Marx, O., Brümmer, C., Neftel, A., 2012. Measuring the biosphere-atmosphere exchange of total reactive nitrogen by eddy covariance. Biogeosciences 9, 4247–4261.

Archibald, S., Kirton, A., Van der Merwe, M.R., Scholes, R., Williams, C.A., Hanan, N., 2009. Drivers of inter-annual variability in Net Ecosystem Exchange in a semi-arid savanna ecosystem, South Africa. Biogeosciences 6, 251–266.

Aurela, M., Lohila, A., Tuovinen, J.-P., Hatakka, J., Riutta, T., Laurila, T., 2009. Carbon dioxide exchange on a northern boreal fen. Boreal Environ. Res. 14, 699.

Baier, W., 1966. Studies on dew formation under semi-arid conditions. Agric. Meteorol. 3, 103–112. https://doi.org/10.1016/0002-1571(66)90008-2

Behera, S.N., Sharma, M., 2011. Degradation of SO2, NO2 and NH3 leading to formation of secondary inorganic aerosols: An environmental chamber study. Atmos. Environ. 45, 4015–4024. https://doi.org/10.1016/j.atmosenv.2011.04.056

Beukes, J.P., Van Zyl, P.G., Venteric, A.D., Josipov, M., Jaars, K., Tiitta, P., Pienaar, J.J., Laakso, L., Vakkari, V., Kulmala, M., 2013. Source region plume characterisation of the interior of South Africa as observed at Welgegund. Clean Air J. Tydskr. Vir Skoon Lug 23, 7–10.

Bleeker, A., Hicks, W.K., Dentener, F., Galloway, J., Erisman, J.W., 2011. N deposition as a threat to the World's protected areas under the Convention on Biological Diversity. Environ. Pollut. 159, 2280–2288.

Borer, E.T., Stevens, C.J., 2022. Nitrogen deposition and climate: an integrated synthesis. Trends Ecol. Evol. 37, 541–552. https://doi.org/10.1016/j.tree.2022.02.013

Bowman, W.D., Cleveland, C.C., Halada, Ľ., Hreško, J., Baron, J.S., 2008. Negative impact of nitrogen deposition on soil buffering capacity. Nat. Geosci. 1, 767–770.

Breuninger, C., Meixner, F.X., Kesselmeier, J., 2013. Field investigations of nitrogen dioxide (NO 2) exchange between plants and the atmosphere. Atmospheric Chem. Phys. 13, 773–790.

Breuninger, C., Oswald, R., Kesselmeier, J., Meixner, F.X., 2011. The dynamic chamber method: trace gas exchange fluxes (NO, NO 2, O 3) between plants and the atmosphere in the laboratory and in the field. Atmospheric Meas. Tech. Discuss. 4, 5183–5274.

Brümmer, C., Marx ,Oliver, Kutsch ,Werner, Ammann ,Christof, Wolff ,Veronika, Flechard ,Christopher., and Freibauer, A., 2013. Fluxes of total reactive atmospheric nitrogen (ΣNr) using eddy covariance above arable land. Tellus B Chem. Phys. Meteorol. 65, 19770. https://doi.org/10.3402/tellusb.v65i0.19770

https://doi.org/10.5194/egusphere-2026-3066
Preprint. Discussion started: 11 June 2026

Butterbach-Bahl, K., Baggs, E.M., Dannenmann, M., Kiese, R., Zechmeister-Boltenstern, S., 2013. Nitrous oxide emissions from soils: how well do we understand the processes and their controls? Philos. Trans. R. Soc. B Biol. Sci. 368.

Chaparro-Suarez, I., Meixner, F., Kesselmeier, J., 2011a. Nitrogen dioxide (NO2) uptake by vegetation controlled by atmospheric concentrations and plant stomatal aperture. Atmos. Environ. 45, 5742–5750.

Chaparro-Suarez, I., Meixner, F., Kesselmeier, J., 2011b. Nitrogen dioxide (NO2) uptake by vegetation controlled by atmospheric concentrations and plant stomatal aperture. Atmos. Environ. 45, 5742–5750.

Chen, S., Chen, B., Wang, S., Sun, L., Shi, H., Liu, Z., Wang, Q., Li, H., Zhu, T., Li, D., Xia, Y., Zhao, Z., Wang, Lunche, Wang, Lizhe, 2023. Spatiotemporal variations of atmospheric nitrogen deposition in China during 2008–2020. Atmos. Environ. 315, 120120. https://doi.org/10.1016/j.atmosenv.2023.120120

Chen, W., Jia, S., Wang, X., Shao, M., Liao, W., Guenther, A., Flechard, C., Yu, P., Zhong, B., Chang, M., Wang, W., Mao, J., Liu, X., Yu, G., Carmichael, G., 2023. Precipitation trend increases the contribution of dry reduced nitrogen deposition. Npj Clim. Atmospheric Sci. 6, 62. https://doi.org/10.1038/s41612-023-00390-7

Cheng, M., Jiang, H., Guo, Z., Zhang, X., Lu, X., 2013. Estimating NO2 dry deposition using satellite data in eastern China. Int. J. Remote Sens. 34, 2548–2565.

Conrad, R., 1994. Compensation concentration as critical variable for regulating the flux of trace gases between soil and atmosphere. Biogeochemistry 27, 155–170.

Cosijn, C. *&Tyson P.D.**, 1996. Stable discontinuities in the atmosphere over South Africa. South Afr. J. Sci. 92, 381–386. https://doi.org/10.10520/AJA00382353_7756

De Lange, A., Naidoo, M., Garland, R.M., Dyson, L.L., 2021. Sensitivity of meteorological variables on planetary boundary layer parameterization schemes in the WRF-ARW model. Atmospheric Res. 247, 105214.

de Vries, W., Erisman, J.W., Spranger, T., Stevens, C.J., van den Berg, L., 2011. Nitrogen as a threat to European terrestrial biodiversity. Eur. Nitrogen Assess. Sources Eff. Policy Perspect. 436–494.

Delaria, E.R., Vieira, M., Cremieux, J., Cohen, R.C., 2018. Measurements of NO and NO 2 exchange between the atmosphere and Quercus agrifolia. Atmospheric Chem. Phys. 18, 14161–14173.

Deng, O., Zhang, S., Deng, L., Lan, T., Luo, L., Gao, X., Zhou, W., 2019. Atmospheric dry nitrogen deposition and its relationship with local land use in a high nitrogen deposition region. Atmos. Environ. 203, 114–120. https://doi.org/10.1016/j.atmosenv.2018.12.037

Dentener, F., Drevet, J., Lamarque, J.F., Bey, I., Eickhout, B., Fiore, A.M., Hauglustaine, D., Horowitz, L.W., Krol, M., Kulshrestha, U.C., Lawrence, M., Galy-Lacaux, C., Rast, S., Shindell, D., Stevenson, D., Van Noije, T., Atherton, C., Bell, N., Bergman, D., Butler, T., Cofala, J., Collins, B., Doherty, R., Ellingsen, K., Galloway, J., Gauss, M., Montanaro, V., Müller, J.F., Pitari, G., Rodriguez, J., Sanderson, M., Solmon, F., Strahan, S., Schultz, M., Sudo, K., Szopa, S., Wild, O., 2006. Nitrogen and sulfur deposition on regional and global scales: A multimodel evaluation. Glob. Biogeochem. Cycles 20. https://doi.org/10.1029/2005GB002672

Donnou, H.E.V., Akpo, A.B., Ossohou, M., Delon, C., Yoboué, V., Laouali, D., Ouafo-Leumbe, M., Van Zyl, P.G., Ndiaye, O., Gardrat, E., 2024. Measurement report: Long-term measurements of surface ozone and trends in semi-natural sub-Saharan African ecosystems. Atmospheric Chem. Phys. 24, 13151–13182.

Duce, R.A., LaRoche, J., Altieri, K., Arrigo, K.R., Baker, A.R., Capone, D., Cornell, S., Dentener, F., Galloway, J., Ganeshram, R.S., 2008. Impacts of atmospheric anthropogenic nitrogen on the open ocean. science 320, 893–897.

Eller, A.S.D., Sparks, J.P., 2006. Predicting leaf-level fluxes of O3 and NO2: the relative roles of diffusion and biochemical processes. Plant Cell Environ. 29, 1742–1750. https://doi.org/10.1111/j.1365-3040.2006.01546.x

Eugster, W., Hesterberg, R., 1996. Transfer resistances of NO2 determined from eddy correlation flux measurements over a litter meadow at a rural site on the swiss plateau. Atmos. Environ. 30, 1247–1254. https://doi.org/10.1016/1352-2310(95)00418-1

Farmer, D., Cohen, R., 2008. Observations of HNO 3, ΣAN, ΣPN and NO 2 fluxes: evidence for rapid HO x chemistry within a pine forest canopy. Atmospheric Chem. Phys. 8, 3899–3917.

Farmer, D., Wooldridge, P., Cohen, R., 2006. Application of thermal-dissociation laser induced fluorescence (TD-LIF) to measurement of HNO 3, Σalkyl nitrates, Σperoxy nitrates, and NO 2 fluxes using eddy covariance. Atmospheric Chem. Phys. 6, 3471–3486.

Farquhar, G.D., Sharkey, T.D., 1982. Stomatal Conductance and Photosynthesis. Annu. Rev. Plant Physiol. 33, 317–345. https://doi.org/10.1146/annurev.pp.33.060182.001533

https://doi.org/10.5194/egusphere-2026-3066
Preprint. Discussion started: 11 June 2026

Feig, G., Mamtimin, B., Meixner, F., 2008. Soil biogenic emissions of nitric oxide from a semi-arid savanna in South Africa. Biogeosciences 5, 1723–1738.

Feng, X., Wang, R., Li, T., Cai, J., Liu, H., Li, H., Jiang, Y., 2024. Plant functional traits modulate the effects of soil acidification on above- and belowground biomass. Biogeosciences 21, 2641–2653. https://doi.org/10.5194/bg-21-2641-2024

Foken, Th., Wichura, B., 1996. Tools for quality assessment of surface-based flux measurements. Agric. For. Meteorol. 78, 83–105. https://doi.org/10.1016/0168-1923(95)02248-1

Fowler, D., Brimblecombe, P., Burrows, J., Heal, M.R., Grennfelt, P., Stevenson, D.S., Jowett, A., Nemitz, E., Coyle, M., Liu, X., Chang, Y., Fuller, G.W., Sutton, M.A., Klimont, Z., Unsworth, M.H., Vieno, M., 2020. A chronology of global air quality. Philos. Trans. R. Soc. Math. Phys. Eng. Sci. 378, 20190314. https://doi.org/10.1098/rsta.2019.0314

Fowler, D., Cape, J., Unsworth, M., 1989. Deposition of atmospheric pollutants on forests. Philos. Trans. R. Soc. Lond. B Biol. Sci. 324, 247–265.

Freiman, M.T., Piketh, S.J., 2003. Air Transport into and out of the Industrial Highveld Region of South Africa. J. Appl. Meteorol. 42, 994–1002. https://doi.org/10.1175/1520-0450(2003)042%3C0994:ATIAOO%3E2.0.CO;2

García-Mata, C., Lamattina, L., 2001. Nitric Oxide Induces Stomatal Closure and Enhances the Adaptive Plant Responses against Drought Stress. Plant Physiol. 126, 1196–1204. https://doi.org/10.1104/pp.126.3.1196

Geddes, J., Murphy, J., 2014. Observations of reactive nitrogen oxide fluxes by eddy covariance above two midlatitude North American mixed hardwood forests. Atmospheric Chem. Phys. 14, 2939–2957.

Gerdel, K., Spielmann, F., Hammerle, A., Wohlfahrt, G., 2017. Eddy covariance carbonyl sulfide flux measurements with a quantum cascade laser absorption spectrometer. Atmospheric Meas. Tech. 10, 3525–3537. https://doi.org/10.5194/amt-10-3525-2017

Geßler, A., Rienks, M., Rennenberg, H., 2002. Stomatal uptake and cuticular adsorption contribute to dry deposition of NH3 and NO2 to needles of adult spruce (Picea abies) trees. New Phytol. 156, 179–194. https://doi.org/10.1046/j.1469-8137.2002.00509.x

Gessler, A., Rienks, M., Rennenberg, H., 2000. NH3 and NO2 fluxes between beech trees and the atmosphere – correlation with climatic and physiological parameters. New Phytol. 147, 539–560. https://doi.org/10.1046/j.1469-8137.2000.00712.x

Giardina, M., Donateo, A., Buffa, P., Contini, D., Cervone, A., Lombardo, C., Rocchi, F., 2019. Atmospheric dry deposition processes of particles on urban and suburban surfaces: Modelling and validation works. Atmos. Environ. 214, 116857. https://doi.org/10.1016/j.atmosenv.2019.116857

Gierens, R.T., Henriksson, S., Josipovic, M., Vakkari, V., van Zyl, P.G., Beukes, J.P., Wood, C.R., O'Connor, E.J., 2019. Observing continental boundary-layer structure and evolution over the South African savannah using a ceilometer. Theor. Appl. Climatol. 136, 333–346.

Goulding, K.W., Bailey, N.J., Bradbury, N.J., Hargreaves, P., Howe, M., Murphy, D.V., Poulton, P.R., Willison, T.W., 1998. Nitrogen deposition and its contribution to nitrogen cycling and associated soil processes. New Phytol. 139, 49–58.

Grace, J., José, J., Meir, P., Miranda, H., Montes, R., 2006. Productivity and carbon fluxes of tropical savannas. J. Biogeogr. 33, 387–400. https://doi.org/10.1111/j.1365-2699.2005.01448.x

Guerrieri, R., Siegwolf, R., Saurer, M., Ripullone, F., Mencuccini, M., Borghetti, M., 2010. Anthropogenic NOx emissions alter the intrinsic water-use efficiency (WUEi) for Quercus cerris stands under Mediterranean climate conditions. Environ. Pollut. 158, 2841–2847. https://doi.org/10.1016/j.envpol.2010.06.017

Gut, A., Scheibe, M., Rottenberger, S., Rummel, U., Welling, M., Ammann, C., Kirkman, G.A., Kuhn, U., Meixner, F.X., Kesselmeier, J., Lehmann, B.E., Schmidt, W., Müller, E., Piedade, M.T.F., 2002. Exchange fluxes of NO2 and O3 at soil and leaf surfaces in an Amazonian rain forest. J. Geophys. Res. Atmospheres 107, LBA 27-1. https://doi.org/10.1029/2001JD000654

Hanson, P., Rott, K., Taylor Jr, G., Gunderson, C., Ross-Todd, B., 1989. NO2 deposition to elements representative of a forest landscape. Atmospheric Environ. 1967 23, 1783–1794.

Harris, G.W., Wienhold, F.G., Zenker, T., 1996. Airborne observations of strong biogenic NO emissions from the Namibian savanna at the end of the dry season. J. Geophys. Res. Atmospheres 101, 23707–23711. https://doi.org/10.1029/96JD01278

https://doi.org/10.5194/egusphere-2026-3066
Preprint. Discussion started: 11 June 2026

Held, G., Mphepya, J., 2000. Wet and dry deposition in South Africa. Presented at the Proceedings, XI Congresso Brasiliero de Meteorologia (CDROM), SBMET, Rio de Janeiro, pp. 16–20.

Hertel, O., Reis, S., Skjoth, C.A., Bleeker, A., Harrison, R., Cape, J.N., Fowler, D., Skiba, U., Simpson, D., Jickells, T., 2011. Nitrogen processes in the atmosphere.

Hicks, B., Baldocchi, D., Meyers, T., Hosker, R., Matt, D., 1987. A preliminary multiple resistance routine for deriving dry deposition velocities from measured quantities. Water. Air. Soil Pollut. 36, 311–330.

Hicks, B.B., Matt, D.R., 1988. Combining biology, chemistry, and meteorology in modeling and measuring dry deposition. J. Atmospheric Chem. 6, 117–131. https://doi.org/10.1007/BF00048335

Horii, C.V., 2002. Tropospheric reactive nitrogen speciation, deposition, and chemistry at Harvard Forest. Harvard University.

Horii, C.V., Munger, J.W., Wofsy, S.C., Zahniser, M., Nelson, D., McManus, J.B., 2004. Fluxes of nitrogen oxides over a temperate deciduous forest. J. Geophys. Res. Atmospheres 109. https://doi.org/10.1029/2003JD004326

Horii, C.V., Zahniser, M.S., Nelson Jr, D.D., McManus, J.B., Wofsy, S.C., 1999. Nitric acid and nitrogen dioxide flux measurements: a new application of tunable diode laser absorption spectroscopy. Presented at the Application of Tunable Diode and Other Infrared Sources for Atmospheric Studies and Industrial Processing Monitoring II, SPIE, pp. 152–161.

Hossain, M.A., Wani, S.H., Bhattacharjee, S., Burritt, D.J., Tran, L.-S.P., 2016. Drought stress tolerance in plants, Volume. Switz. Springer 1, 105–143.

Jaars, K., Beukes, J., Van Zyl, P., Venter, A., Josipovic, M., Pienaar, J., Vakkari, V., Aaltonen, H., Laakso, H., Kulmala, M., 2014. Ambient aromatic hydrocarbon measurements at Welgegund, South Africa. Atmospheric Chem. Phys. 14, 7075–7089.

Jaars, K., Van Zyl, P.G., Beukes, J.P., Josipovic, M., Venter, A.D., Knoetze, L., Cilliers, D.P., Siebert, S.J., Laakso, L., 2016. Measurements of biogenic volatile organic compounds at a grazed savannah grassland agricultural landscape in South Africa.

Jia, Y., Yu, G., Gao, Y., He, N., Wang, Q., Jiao, C., Zuo, Y., 2016. Global inorganic nitrogen dry deposition inferred from ground- and space-based measurements. Sci. Rep. 6, 19810. https://doi.org/10.1038/srep19810

Jiang, W., Shen, J., Li, Y., Wang, J., Gong, D., Zhu, X., Liu, X., Liu, J., Reis, S., Zhu, Q., Wu, J., 2024. Contrasting change trends in dry and wet nitrogen depositions during 2011 to 2020: Evidence from an agricultural catchment in subtropical Central China. Sci. Total Environ. 907, 168094. https://doi.org/10.1016/j.scitotenv.2023.168094

Jin, S., Kong, L., Yang, K., Wang, C., Xia, L., Wang, Y., Tan, J., Wang, L., 2022. Combined effects of high relative humidity and ultraviolet irradiation: Enhancing the production of gaseous NO2 from the photolysis of NH4NO3. Sci. Total Environ. 838, 156480. https://doi.org/10.1016/j.scitotenv.2022.156480

Josipovic, M., Annegarn, H.J., Kneen, M.A., Pienaar, J.J., Piketh, S.J., 2011. Atmospheric dry and wet deposition of sulphur and nitrogen species and assessment of critical loads of acidic deposition exceedance in South Africa. South Afr. J. Sci. 107, 01–10.

Kai, R.F., Scholes, M.C., Piketh, S.J., Scholes, R.J., 2022. Analysis of the first surface nitrogen dioxide concentration observations over the South African Highveld derived from the Pandora-2s instrument. Clean Air J. 32, 1–11.

Kai-Sikhakhane, R.F., Scholes, M.C., Piketh, S.J., van Geffen, J., Garland, R.M., Havenga, H., Scholes, R.J., 2024. Assessing Nitrogen Dioxide in the Highveld Troposphere: Pandora Insights and TROPOMI Sentinel-5P Evaluation. Atmosphere 15. https://doi.org/10.3390/atmos15101187

Kang, R., Huang, K., Gao, T., Mulder, J., Duan, L., Wang, C., Ke, P., Yao, M., Su, C., Li, J., Zhu, W., Zhu, J., Fang, Y., 2023. Forest Canopy Acts as an Atmospheric NOx Sink: Results From Micrometeorological Flux Measurements. J. Geophys. Res. Atmospheres 128, e2022JD037729. https://doi.org/10.1029/2022JD037729

Karl, T., Graus, M., Striednig, M., Lamprecht, C., Hammerle, A., Wohlfahrt, G., Held, A., von der Heyden, L., Deventer, M.J., Krismer, A., Haun, C., Feichter, R., Lee, J., 2017. Urban eddy covariance measurements reveal significant missing NOx emissions in Central Europe. Sci. Rep. 7, 2536. https://doi.org/10.1038/s41598-017-02699-9

Ke, P., Ge, X., Yu, C., Yang, D., Kang, R., Huang, Y., Duan, L., 2025. Field investigation of leaf-level NO and NO2 exchange between atmosphere and mature Pinus massoniana in a subtropical forest. J. Geophys. Res. Atmospheres 130, e2024JD040905.

Ke, P., Yu, Q., Luo, Y., Kang, R., Duan, L., 2020. Fluxes of nitrogen oxides above a subtropical forest canopy in China. Sci. Total Environ. 715, 136993.

https://doi.org/10.5194/egusphere-2026-3066
Preprint. Discussion started: 11 June 2026

Kok, L., Van Zyl, P., Beukes, J., Swartz, J., Burger, R., Ellis, S., Josipovic, M., Vakkari, V., Laakso, L., Kulmala, M., 2021. Chemical composition of rain at a regional site on the South African Highveld. Water SA 47, 326–337.

Kopáček, J., Posch, M., Hejzlar, J., Oulehle, F., Volková, A., 2012. An elevation-based regional model for interpolating sulphur and nitrogen deposition. Atmos. Environ. 50, 287–296. https://doi.org/10.1016/j.atmosenv.2011.12.017

Korhonen, K., Giannakaki, E., Mielonen, T., Pfüller, A., Laakso, L., Vakkari, V., Baars, H., Engelmann, R., Beukes, J., Van Zyl, P., 2014. Atmospheric boundary layer top height in South Africa: measurements with lidar and radiosonde compared to three atmospheric models. Atmospheric Chem. Phys. 14, 4263–4278.

Laakso, L., Vakkari, V., Virkkula, A., Laakso, H., Backman, J., Kulmala, M., Beukes, J., Van Zyl, P., Tiitta, P., Josipovic, M., 2012. South African EUCAARI measurements: seasonal variation of trace gases and aerosol optical properties. Atmospheric Chem. Phys. 12, 1847–1864.

Laban, T.L., Van Zyl, P.G., Beukes, J.P., Vakkari, V., Jaars, K., Borduas-Dedekind, N., Josipovic, M., Thompson, A.M., Kulmala, M., Laakso, L., 2018. Seasonal influences on surface ozone variability in continental South Africa and implications for air quality. Atmospheric Chem. Phys. 18, 15491–15514.

Lestari, P., Oskouie, A.K., Noll, K.E., 2003. Size distribution and dry deposition of particulate mass, sulfate and nitrate in an urban area. Atmos. Environ. 37, 2507–2516. https://doi.org/10.1016/S1352-2310(03)00151-1

Li, J.S., Chen, W., Fischer, H., 2013. Quantum Cascade Laser Spectrometry Techniques: A New Trend in Atmospheric Chemistry. Appl. Spectrosc. Rev. 48, 523–559. https://doi.org/10.1080/05704928.2012.757232

Li, S., Bowker, M.A., Xiao, B., 2021. Biocrusts enhance non-rainfall water deposition and alter its distribution in dryland soils. J. Hydrol. 595, 126050. https://doi.org/10.1016/j.jhydrol.2021.126050

Lourens, A.S., Fourie, G.D., Burger, J.W., Pienaar, J.J., Read, C.E., Jordaan, J.H., Van Zyl, P.G., Beukes, J.P., 2011. Spatial and temporal assessment of gaseous pollutants in the Highveld of South Africa. South Afr. J. Sci. 107, 1–8.

Lu, X., Mao, Q., Gilliam, F.S., Luo, Y., Mo, J., 2014. Nitrogen deposition contributes to soil acidification in tropical ecosystems. Glob. Change Biol. 20, 3790–3801.

Maluleke, A., 2024. Exchange of Carbon dioxide, Water and Energy in South African semi-arid ecosystems.

Maluleke, A., Feig, G., Brümmer, C., Jaars, K., Hamilton, T., Midgley, G., 2025. Paired eddy covariance site reveals consistent net C sinks over three growing seasons in an African arid and grassy shrubland. Agric. For. Meteorol. 372, 110705.

Mariraj Mohan, S., 2016. An overview of particulate dry deposition: measuring methods, deposition velocity and controlling factors. Int. J. Environ. Sci. Technol. 13, 387–402. https://doi.org/10.1007/s13762-015-0898-7

Maritz, P., Beukes, J.P., Van Zyl, P.G., Conradie, E.H., Liousse, C., Galy-Lacaux, C., Castéra, P., Ramandh, A., Mkhatshwa, G., Venter, A.D., 2015. Spatial and temporal assessment of organic and black carbon at four sites in the interior of South Africa. Clean Air J. 25, 20–20.

Min, K.-E., Pusede, S., Browne, E., LaFranchi, B., Cohen, R., 2014. Eddy covariance fluxes and vertical concentration gradient measurements of NO and NO 2 over a ponderosa pine ecosystem: observational evidence for within-canopy chemical removal of NO x. Atmospheric Chem. Phys. 14, 5495–5512.

Mompati, M.K., Piketh, S.J., Curtis, C., Van Zyl, P.G., 2019. atmospheric deposition of Sulphur and Nitrogen over Eastern South africa.

Mphepya, J.N., 2002. Atmospheric deposition characteristics of sulphur and nitrogen compounds in South Africa.

Muselli, M., Beysens, D., 2021. Mapping past, present and future dew and rain water resources for biocrust evolution in southern Africa. J. Hydrol. Hydromech. 69, 400–420.

Nowlan, C.R., Martin, R.V., Philip, S., Lamsal, L.N., Krotkov, N.A., Marais, E.A., Wang, S., Zhang, Q., 2014. Global dry deposition of nitrogen dioxide and sulfur dioxide inferred from space-based measurements. Glob. Biogeochem. Cycles 28, 1025–1043. https://doi.org/10.1002/2014GB004805

Okamura, S., Ueyama, M., Takahashi, K., 2024. Temporal and spatial variations in NO2 fluxes by tall tower eddy covariance measurements over a dense urban center in Sakai, Japan. Atmos. Environ. 339, 120870. https://doi.org/10.1016/j.atmosenv.2024.120870

Papale, D., Reichstein, M., Aubinet, M., Canfora, E., Bernhofer, C., Kutsch, W., Longdoz, B., Rambal, S., Valentini, R., Vesala, T., 2006. Towards a standardized processing of Net Ecosystem Exchange measured with eddy covariance technique: algorithms and uncertainty estimation. Biogeosciences 3, 571–583.

Phala, R.N., 2015. Using an Inferential Model to Estimate Dry Deposition of SO2and NOX (As NO2) in Lephalale in the Waterberg-Bojanala Priority Area. University of the Witwatersrand, Johannesburg (South Africa).

https://doi.org/10.5194/egusphere-2026-3066
Preprint. Discussion started: 11 June 2026

Pilegaard, K., HummelshØj, P., Jensen, N.O., 1998. Fluxes of ozone and nitrogen dioxide measured by Eddt correlation over a harvested wheat field. Atmos. Environ. 32, 1167–1177. https://doi.org/10.1016/S1352-2310(97)00194-5

Raivonen, M., Vesala, T., Pirjola, L., Altimir, N., Keronen, P., Kulmala, M., Hari, P., 2009. Compensation point of NOx exchange: Net result of NOx consumption and production. Agric. For. Meteorol. 149, 1073–1081.

Räsänen, M., Aurela, M., Vakkari, V., Beukes, J.P., Tuovinen, J.-P., Van Zyl, P.G., Josipovic, M., Venter, A.D., Jaars, K., Siebert, S.J., 2017. Carbon balance of a grazed savanna grassland ecosystem in South Africa. Biogeosciences 14, 1039–1054.

Rodriguez-Caballero, E., Belnap, J., Büdel, B., Crutzen, P.J., Andreae, M.O., Pöschl, U., Weber, B., 2018. Dryland photoautotrophic soil surface communities endangered by global change. Nat. Geosci. 11, 185–189.

Rummel, U., Ammann, C., Gut, A., Meixner, F., Andreae, M., 2002. Eddy covariance measurements of nitric oxide flux within an Amazonian rain forest. J. Geophys. Res. 107. https://doi.org/10.1029/2001jd000520

Sadanaga, Y., Matsumoto, J., Kajii, Y., 2003. Photochemical reactions in the urban air: Recent understandings of radical chemistry. J. Photochem. Photobiol. C Photochem. Rev. 4, 85–104.

Saylor, R.D., Baker ,Barry D., Lee ,Pius, Tong ,Daniel, Pan ,Li, and Hicks, B.B., 2019. The particle dry deposition component of total deposition from air quality models: right, wrong or uncertain? Tellus B Chem. Phys. Meteorol. 71, 1550324. https://doi.org/10.1080/16000889.2018.1550324

Schaufler, G., Kitzler, B., Schindlbacher, A., Skiba, U., Sutton, M., Zechmeister-Boltenstern, S., 2010. Greenhouse gas emissions from European soils under different land use: effects of soil moisture and temperature. Eur. J. Soil Sci. 61, 683–696.

Schwede, D.B., Simpson, D., Tan, J., Fu, J.S., Dentener, F., Du, E., deVries, W., 2018. Spatial variation of modelled total, dry and wet nitrogen deposition to forests at global scale. Environ. Pollut. 243, 1287–1301. https://doi.org/10.1016/j.envpol.2018.09.084

Segakweng, C.K., van Zyl, P.G., Liousse, C., Beukes, J.P., Swartz, J.-S., Gardrat, E., Dias-Alves, M., Burger, R.P., Piketh, S.J., 2022. Measurement report: Size-resolved chemical characterisation of aerosols in low-income urban settlements in South Africa. Atmospheric Chem. Phys. 22, 10291–10317.

Shang, F., Liu, M., Song, Y., Lu, X., Zhang, Q., Matsui, H., Liu, L., Ding, A., Huang, X., Liu, X., Cao, J., Wang, Z., Dai, Y., Kang, L., Cai, X., Zhang, H., Zhu, T., 2024. Substantial nitrogen abatement accompanying decarbonization suppresses terrestrial carbon sinks in China. Nat. Commun. 15, 7738. https://doi.org/10.1038/s41467-024-52152-5

Sparks, J.P., Monson, R.K., Sparks, K.L., Lerdau, M., 2001. Leaf uptake of nitrogen dioxide (NO 2) in a tropical wet forest: implications for tropospheric chemistry. Oecologia 127, 214–221.

Stella, P., Kortner, M., Ammann, C., Foken, T., Meixner, F.X., Trebs, I., 2013. Measurements of nitrogen oxides and ozone fluxes by eddy covariance at a meadow: evidence for an internal leaf resistance to NO 2. Biogeosciences 10, 5997–6017.

Stevens, C.J., Manning, P., van den Berg, L.J.L., de Graaf, M.C.C., Wamelink, G.W.W., Boxman, A.W., Bleeker, A., Vergeer, P., Arroniz-Crespo, M., Limpens, J., Lamers, L.P.M., Bobbink, R., Dorland, E., 2011. Ecosystem responses to reduced and oxidised nitrogen inputs in European terrestrial habitats. Environ. Pollut. 159, 665–676. https://doi.org/10.1016/j.envpol.2010.12.008

Stewart, D., Taylor, C., Reeves, C., McQuaid, J., 2008. Biogenic nitrogen oxide emissions from soils: impact on NO x and ozone over west Africa during AMMA (African Monsoon Multidisciplinary Analysis): observational study. Atmospheric Chem. Phys. 8, 2285–2297.

Stull, R.B., 2012. An introduction to boundary layer meteorology. Springer Science & Business Media.

Teklemariam, T.A., Sparks, J.P., 2006. Leaf fluxes of NO and NO2 in four herbaceous plant species: The role of ascorbic acid. Atmos. Environ. 40, 2235–2244. https://doi.org/10.1016/j.atmosenv.2005.12.010

Thoene, B., Rennenberg, H., Weber, P., 1996. Absorption of atmospheric NO2 by spruce (Picea abies) trees. New Phytol. 134, 257–266. https://doi.org/10.1111/j.1469-8137.1996.tb04630.x

Thomas, C., Foken, T., 2002. P2. 3 RE-EVALUATION OF INTEGRAL TURBULENCE CHARACTERISTICS AND THEIR PARAMETERISATIONS. Presented at the Symposium on Boundary Layers and Turbulence, American Meteorological Society, p. 129.

https://doi.org/10.5194/egusphere-2026-3066
Preprint. Discussion started: 11 June 2026

Trebs, I., Lara, L., Zeri, L., Gatti, L.V., Artaxo, P., Dlugi, R., Slanina, J., Andreae, M., Meixner, F.X., 2006. Dry and wet deposition of inorganic nitrogen compounds to a tropical pasture site (Rondônia, Brazil). Atmospheric Chem. Phys. 6, 447–469.

Tuzson, B., Hiller, R.V., Zeyer, K., Eugster, W., Neftel, A., Ammann, C., Emmenegger, L., 2010. Field intercomparison of two optical analyzers for CH 4 eddy covariance flux measurements. Atmospheric Meas. Tech. 3, 1519–1531.

Tyson, P., Garstang, M., Swap, R., 1996. Large-scale recirculation of air over southern Africa. J. Appl. Meteorol. 35, 2218–2236.

Vakkari, V., Kerminen, V.-M., Beukes, J.P., Tiitta, P., van Zyl, P.G., Josipovic, M., Venter, A.D., Jaars, K., Worsnop, D.R., Kulmala, M., Laakso, L., 2014. Rapid changes in biomass burning aerosols by atmospheric oxidation. Geophys. Res. Lett. 41, 2644–2651. https://doi.org/10.1002/2014GL059396

Valentini, R., Arneth, A., Bombelli, A., Castaldi, S., Cazzolla Gatti, R., Chevallier, F., Ciais, P., Grieco, E., Hartmann, J., Henry, M., 2014. A full greenhouse gases budget of Africa: synthesis, uncertainties, and vulnerabilities. Biogeosciences 11, 381–407.

van der A, R.J., Eskes, H.J., Boersma, K.F., van Noije, T.P.C., Van Roozendael, M., De Smedt, I., Peters, D.H.M.U., Meijer, E.W., 2008. Trends, seasonal variability and dominant NOx source derived from a ten year record of NO2 measured from space. J. Geophys. Res. Atmospheres 113. https://doi.org/10.1029/2007JD009021

Van der Walt, A.J., Fitchett, J.M., 2020. Statistical classification of South African seasonal divisions on the basis of daily temperature data. South Afr. J. Sci. 116, 1–15.

Venter, A.D., Vakkari, V., Beukes, J.P., van Zyl, P.G., Laakso, H., Mabaso, D., Tiitta, P., Josipovic, M., Kulmala, M., Pienaar, J.J., Laakso, L., 2012. An air quality assessment in the industrialised western Bushveld Igneous Complex, South Africa. South Afr. J. Sci. 108, 1–10.

Venter, M., 2020. Aerosol optical properties at a savannah grassland site in South Africa.

Vizcaino, P., Lavalle, C., 2018. Development of European NO2 Land Use Regression Model for present and future exposure assessment: Implications for policy analysis. Environ. Pollut. 240, 140–154.

Wada, R., Yonemura, S., Tani, A., Kajino, M., 2023. Exchanges of O3, NO, and NO2 between forest ecosystems and the atmosphere. J. Agric. Meteorol. 79, 38–48.

Wang, W., Ganzeveld, L., Rossabi, S., Hueber, J., Helmig, D., 2020. Measurement report: Leaf-scale gas exchange of atmospheric reactive trace species (NO2, NO, O3) at a northern hardwood forest in Michigan. Atmospheric Chem. Phys. 20, 11287–11304. https://doi.org/10.5194/acp-20-11287-2020

Wang, X., Wang, L., Shangguan, Z., 2016. Leaf Gas Exchange and Fluorescence of Two Winter Wheat Varieties in Response to Drought Stress and Nitrogen Supply. PLOS ONE 11, e0165733. https://doi.org/10.1371/journal.pone.0165733

Weathers, K.C., Simkin, S.M., Lovett, G.M., Lindberg, S.E., 2006. EMPIRICAL MODELING OF ATMOSPHERIC DEPOSITION IN MOUNTAINOUS LANDSCAPES. Ecol. Appl. 16, 1590–1607. https://doi.org/10.1890/1051-0761(2006)016%5B1590:EMOADI%5D2.0.CO;2

Wesely, M.L., 2007. Parameterization of surface resistances to gaseous dry deposition in regional-scale numerical models. Atmos. Environ. 41, 52–63. https://doi.org/10.1016/j.atmosenv.2007.10.058

Wesely, M.L., 1989. Parameterization of surface resistances to gaseous dry deposition in regional-scale numerical models. Atmospheric Environ. 1967 23, 1293–1304. https://doi.org/10.1016/0004-6981(89)90153-4

Wesely, M.L., Hicks, B.B., 2000. A review of the current status of knowledge on dry deposition. Atmos. Environ. 34, 2261–2282. https://doi.org/10.1016/S1352-2310(99)00467-7

World Meteorological Organization, 2017. WMO Global Atmosphere Watch (GAW) Implementation Plan: 2016–2023.

Wu, Z., Boke-Olén, N., Fensholt, R., Ardö, J., Eklundh, L., Lehsten, V., 2018. Effect of climate dataset selection on simulations of terrestrial GPP: Highest uncertainty for tropical regions. PLoS One 13, e0199383.

Zhang, L., Brook, J., Vet, R., 2003. A revised parameterization for gaseous dry deposition in air-quality models.

Zhang, L., Brook, J.R., Vet, R., Wiebe, A., Mihele, C., Shaw, M., O'Brien, J.M., Iqbal, S., 2005. Estimation of contributions of NO2 and PAN to total atmospheric deposition of oxidized nitrogen across Eastern Canada. Atmos. Environ. 39, 7030–7043. https://doi.org/10.1016/j.atmosenv.2005.08.023

Zhang, L., Moran, M.D., Makar, P.A., Brook, J.R., Gong, S., 2002. Modelling gaseous dry deposition in AURAMS: a unified regional air-quality modelling system. Atmos. Environ. 36, 537–560.

https://doi.org/10.5194/egusphere-2026-3066
Preprint. Discussion started: 11 June 2026

Zhang, L., Vet, R., O'Brien, J.M., Mihele, C., Liang, Z., Wiebe, A., 2009. Dry deposition of individual nitrogen species at eight Canadian rural sites. J. Geophys. Res. Atmospheres 114. https://doi.org/10.1029/2008JD010640

Zhou, K., Zhao, Y., Zhang, L., Xi, M., 2021. Declining dry deposition of NO2 and SO2 with diverse spatiotemporal patterns in China from 2013 to 2018. Atmos. Environ. 262, 118655. https://doi.org/10.1016/j.atmosenv.2021.118655